

---

**Ligand Dechelation effect on a [Co(tpy)<sub>2</sub>]<sup>2+</sup> Scaffold towards  
Electro-catalytic Proton and Water Reduction**

---

# SUPPORTING INFORMATION

KARUNAMAY MAJEE AND SUMANTA KUMAR PADHI

Department of Applied Chemistry, Indian Institute of Technology (ISM), Dhanbad,  
Jharkhand, INDIA, 826 004

## Supporting Information

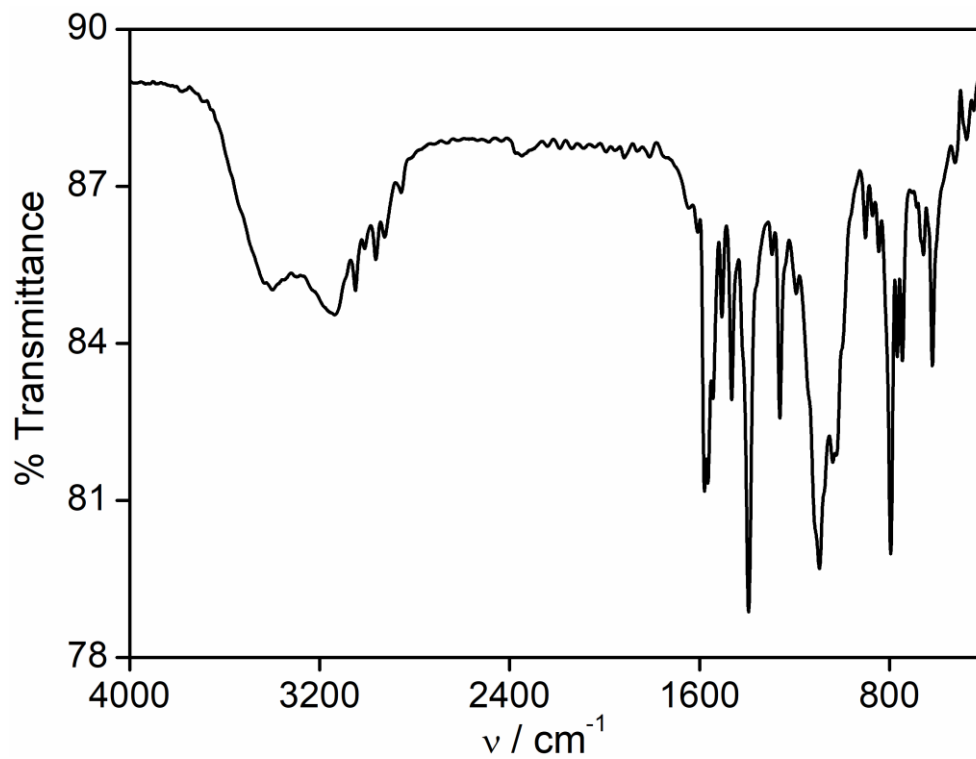


**Figure S1.** IR spectrum of the ligand 4QI-tpy

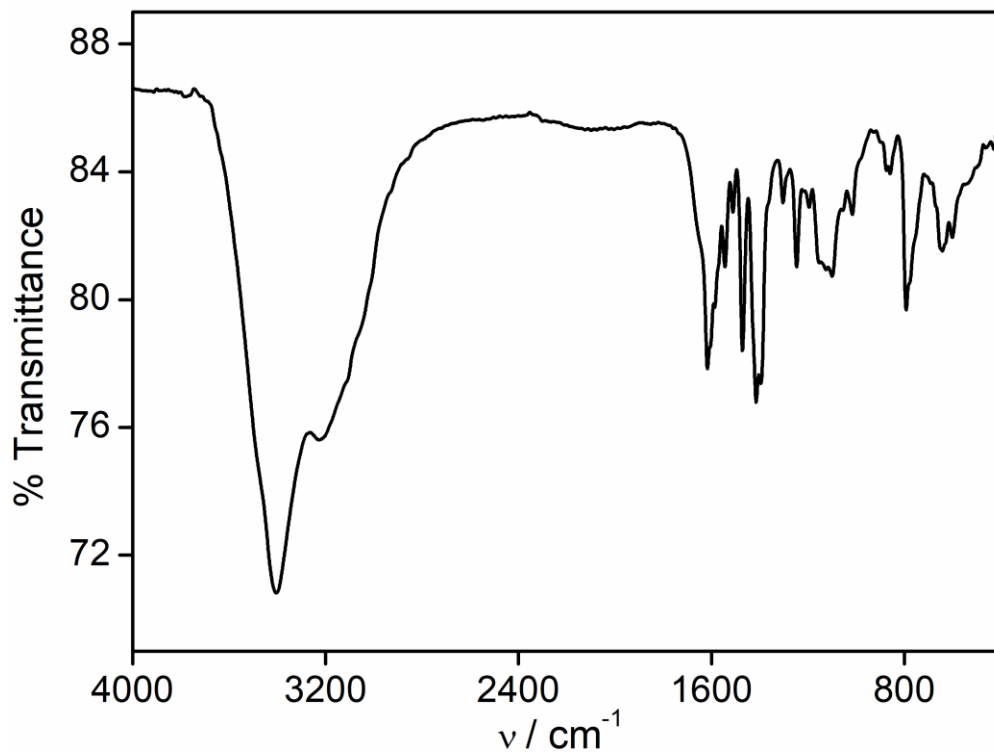


**Figure S2.** IR spectrum of the [Co(4QI-tpy)<sub>2</sub>]Cl<sub>2</sub> complex.

## Supporting Information

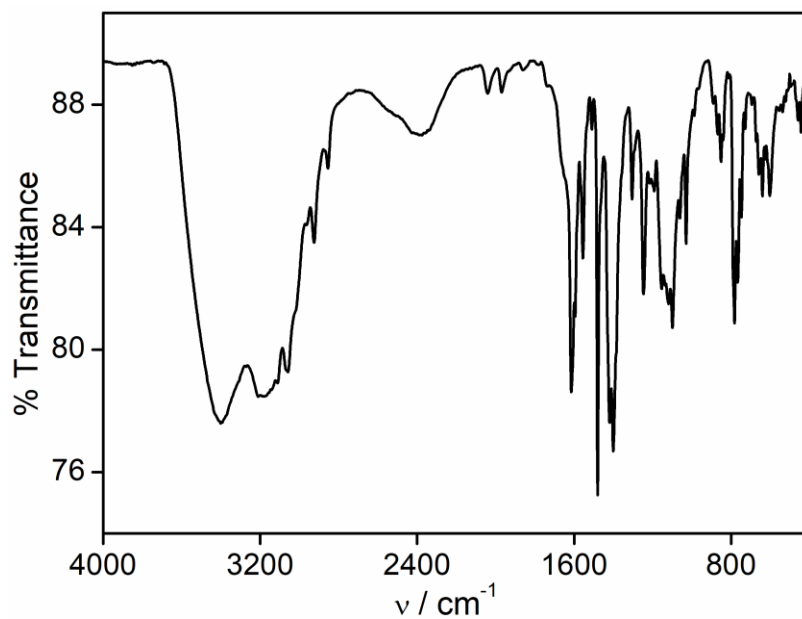


**Figure S3.** IR spectrum of the  $[\text{Co}(\text{4Ql-tpy})_2](\text{PF}_6)_3$  complex.

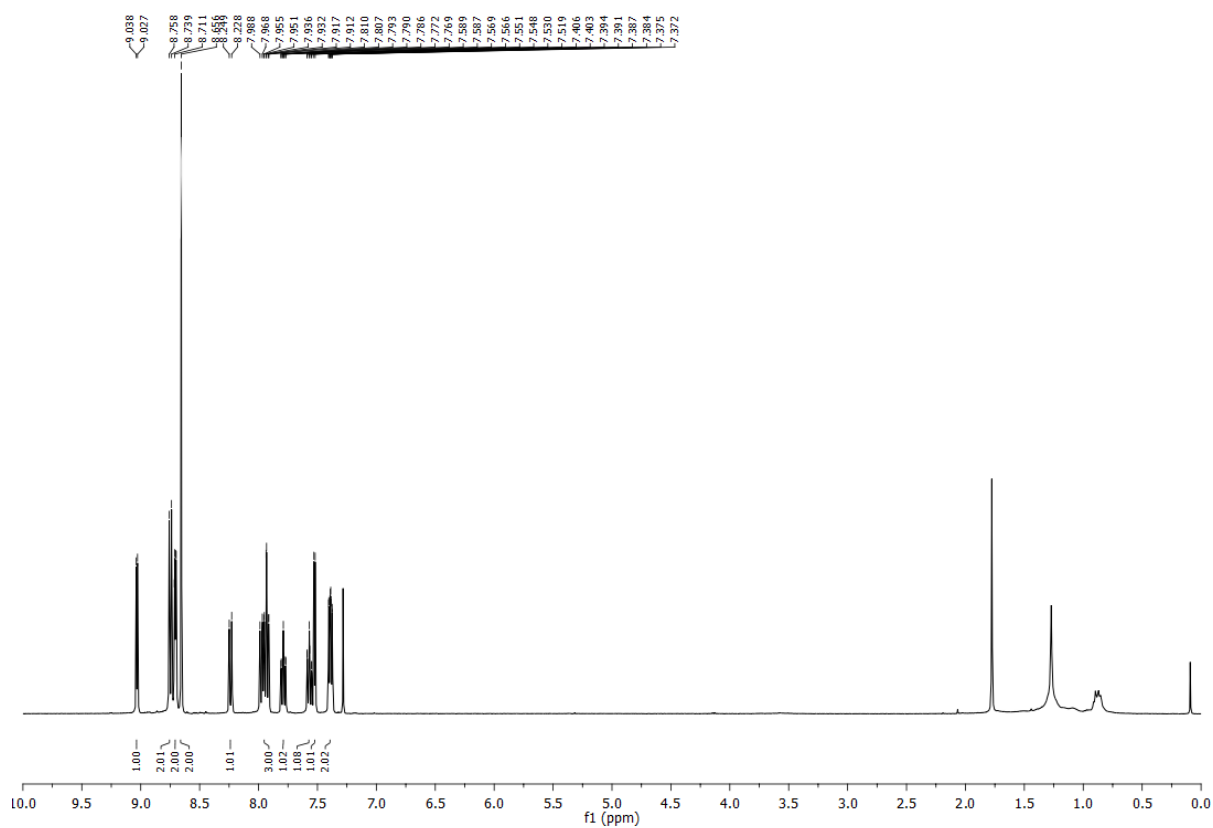


**Figure S4a.**  $^1\text{H}$  NMR spectrum of the ligand 4Ql-tpy in  $\text{CDCl}_3$

## Supporting Information

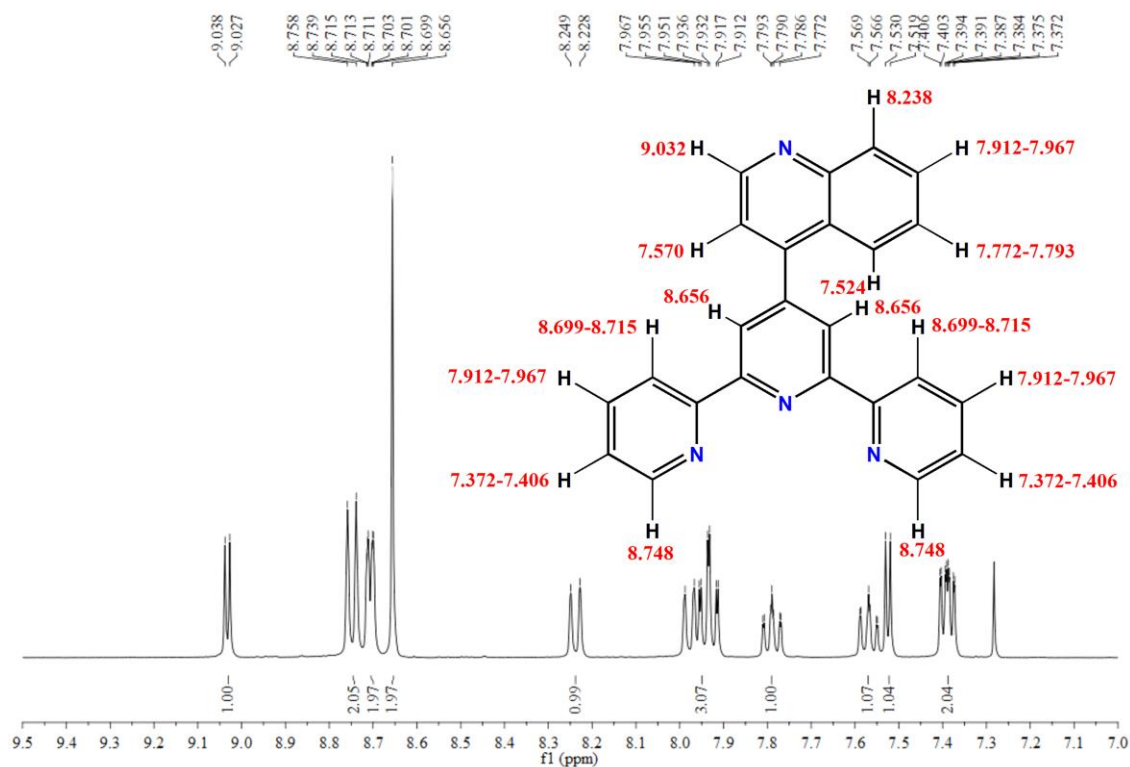


**Figure S4b.**  $^1\text{H}$  NMR spectrum of the ligand 4QI-tpy in  $\text{CDCl}_3$  (Inset is the interpretation).

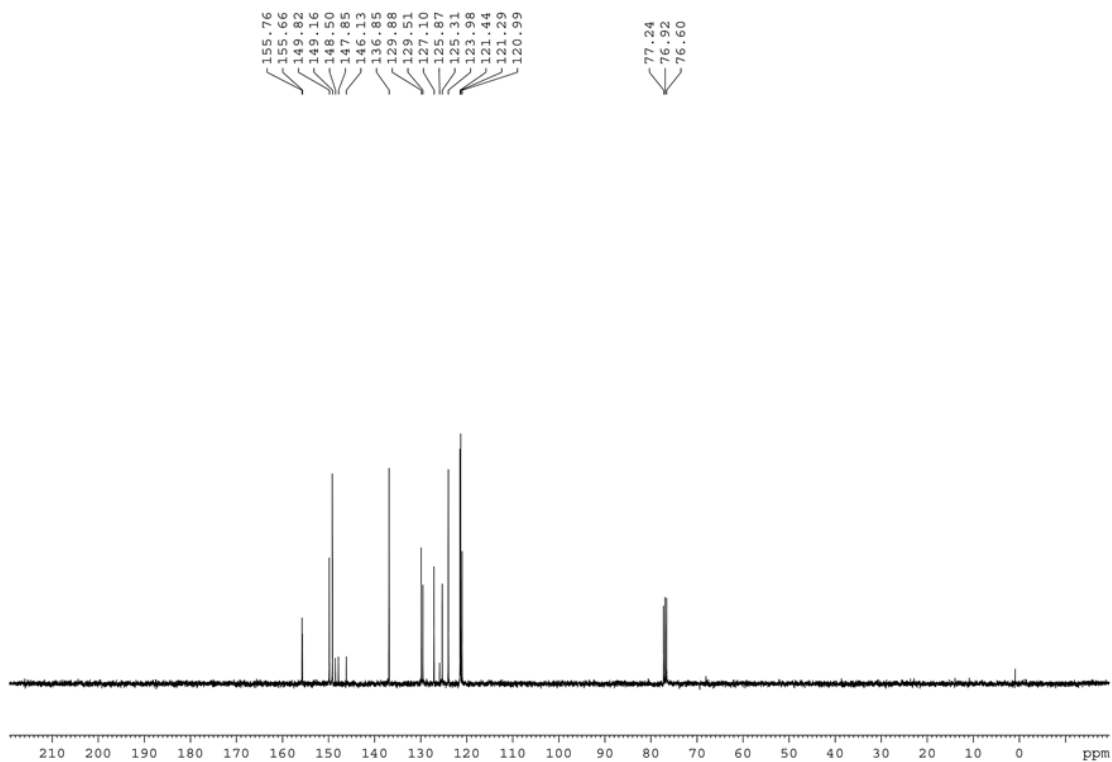


**Figure S5.**  $^{13}\text{C}$  NMR spectrum of ligand 4QI-tpy in  $\text{CDCl}_3$

## Supporting Information

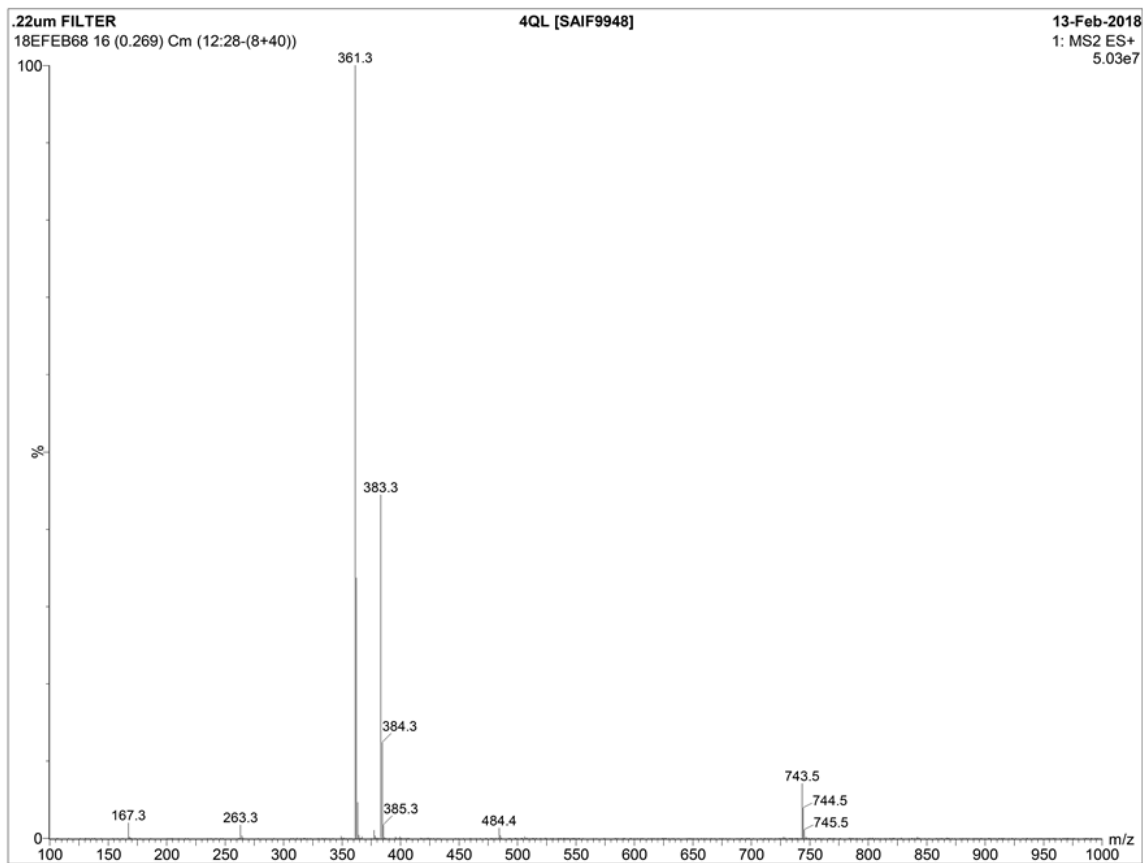


**Figure S6.** ESI-Mass spectrum of ligand 4Ql-tpy in methanol.

## Supporting Information

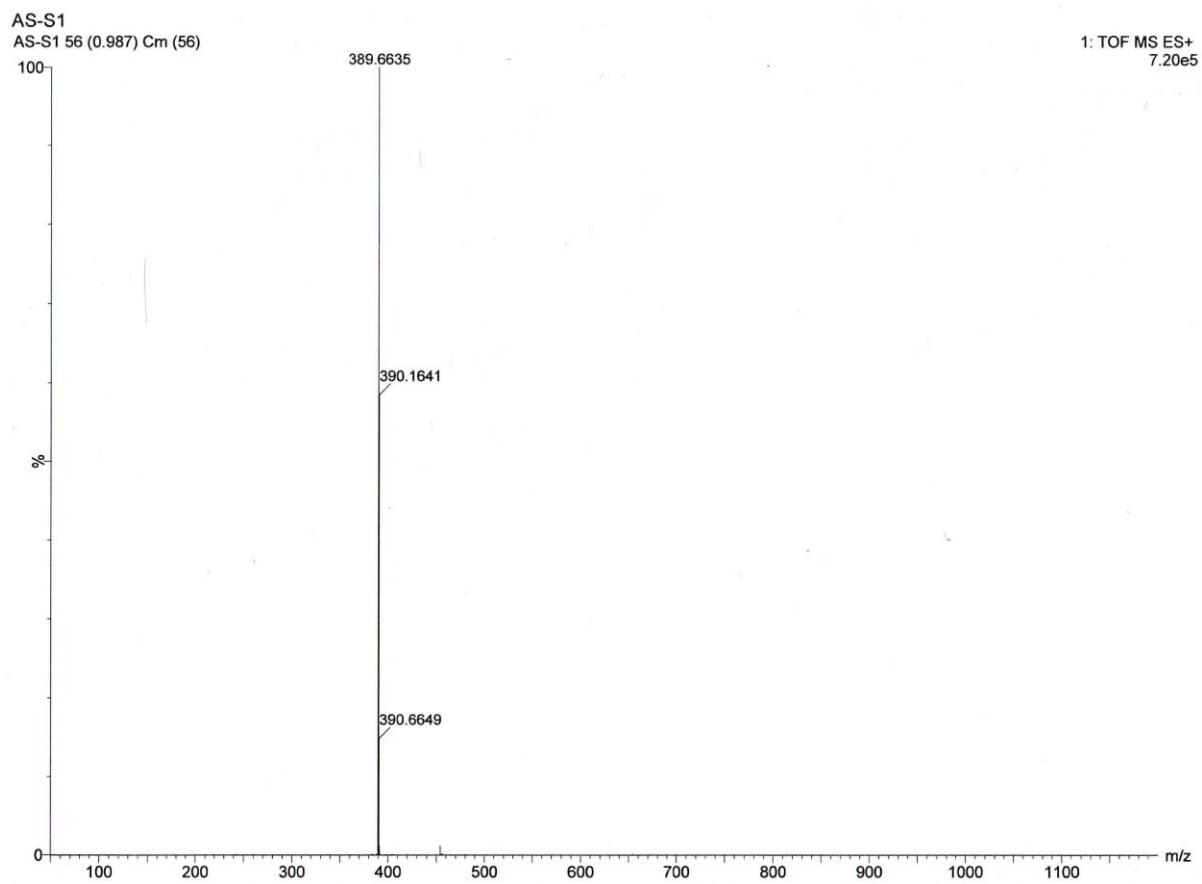


**Figure S7a.** ESI-Mass spectrum of the  $[\text{Co}(\text{4Ql-tpy})_2]\text{Cl}_2$  complex in methanol.

## Supporting Information

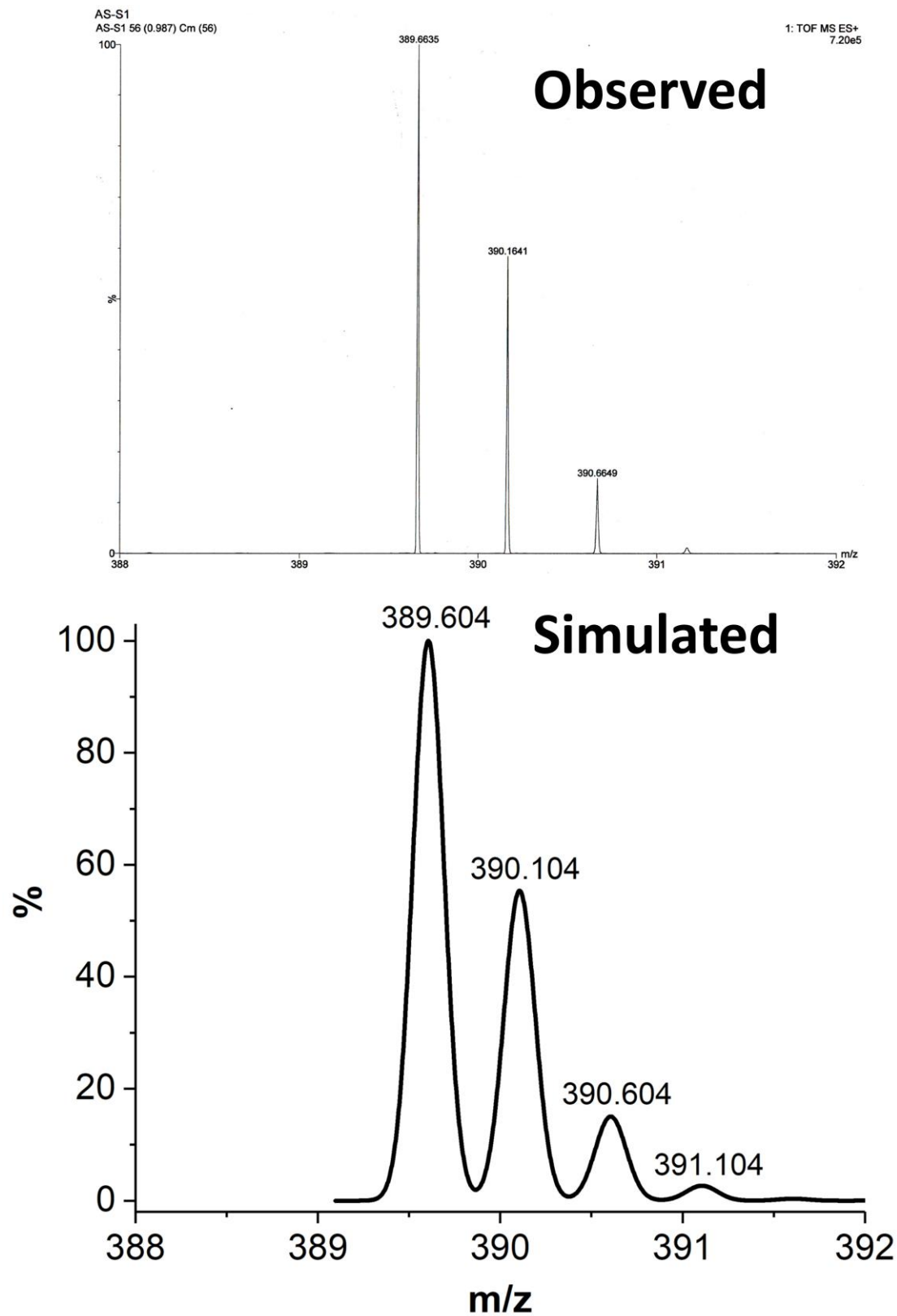


**Figure S7b.** ESI-Mass spectrum of the  $[\text{Co}(4\text{Q1-tpy})_2]\text{Cl}_2$  complex in methanol (Top: Observed; Bottom: Simulated).

# Supporting Information

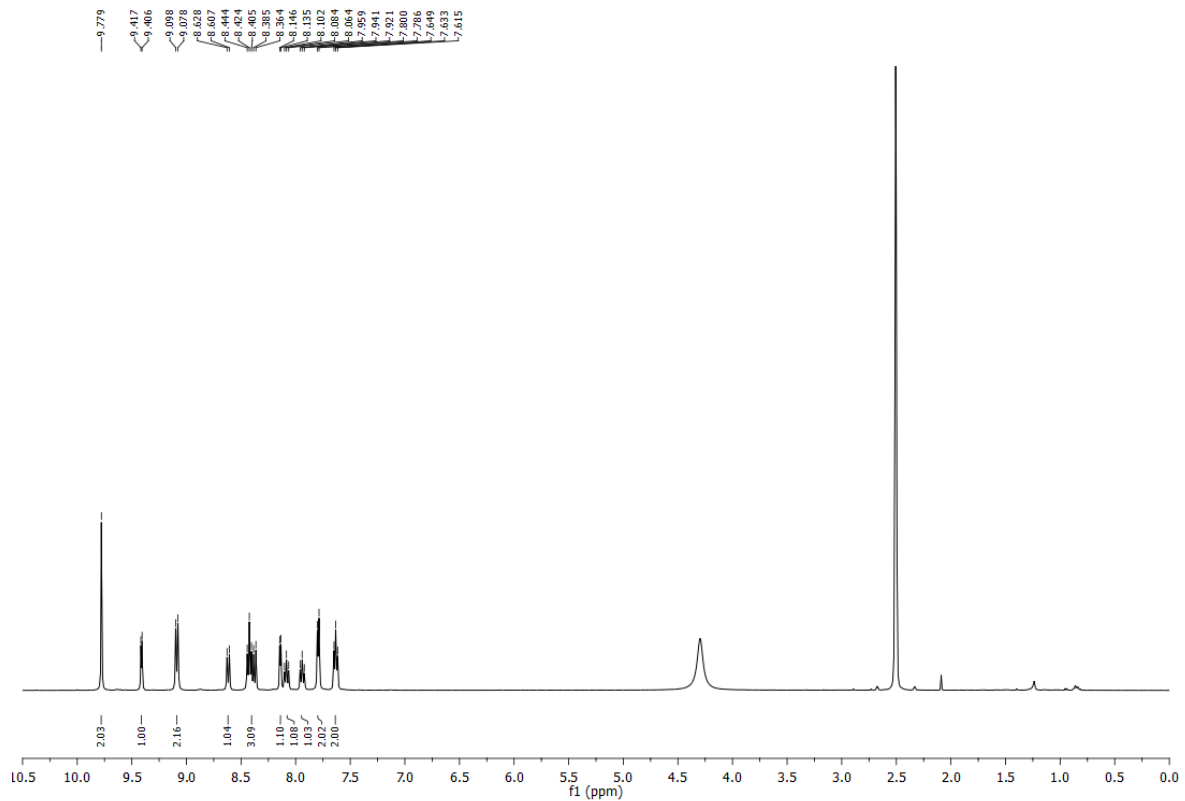


**Figure S8a.**  $^1\text{H}$  NMR spectrum of  $[\text{Co}(\text{4QI-tpy})_2](\text{PF}_6)_3$  complex in  $\text{DMSO-D}_6$ .

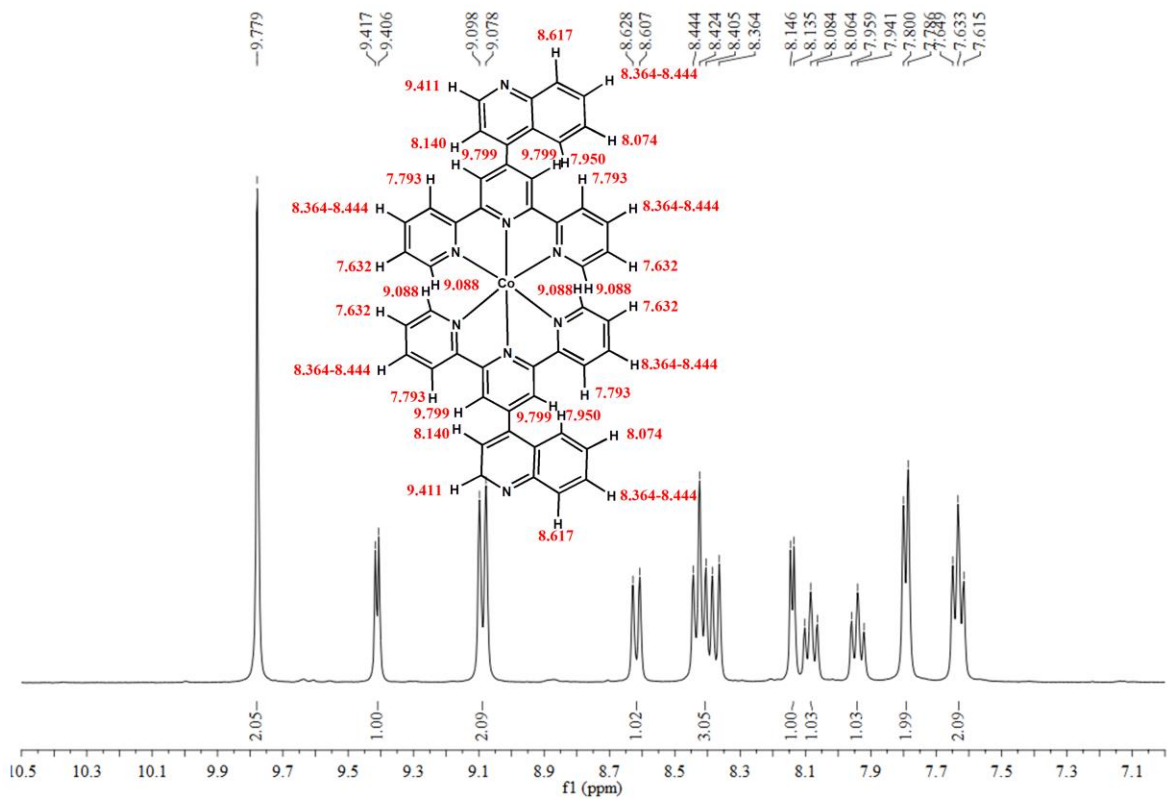


**Figure S8b.**  $^1\text{H}$  NMR spectrum of  $[\text{Co}(\text{4QI-tpy})_2](\text{PF}_6)_3$  complex in  $\text{DMSO-D}_6$ .

## Supporting Information

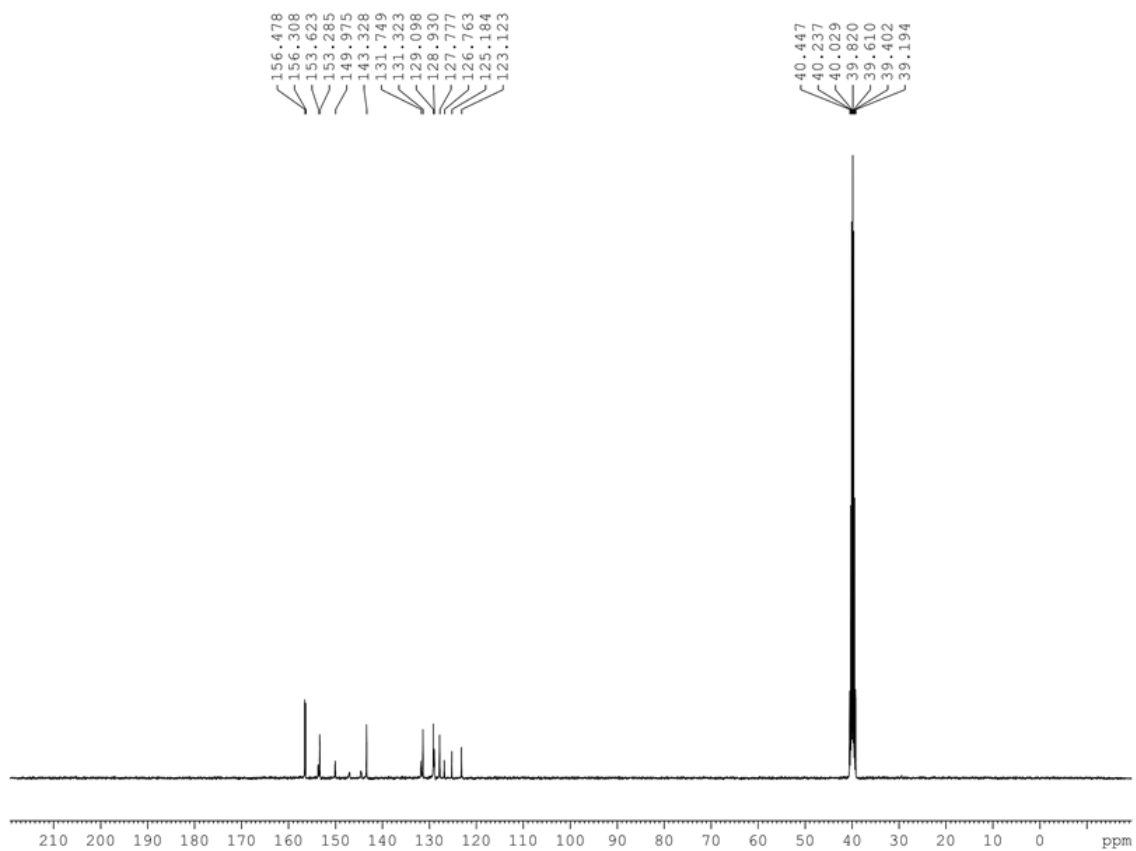


**Figure S9.**  $^{13}\text{C}$  NMR spectrum of  $[\text{Co}(\text{4Ql-tpy})_2](\text{PF}_6)_3$  complex in  $\text{DMSO-D}_6$ .

## Supporting Information

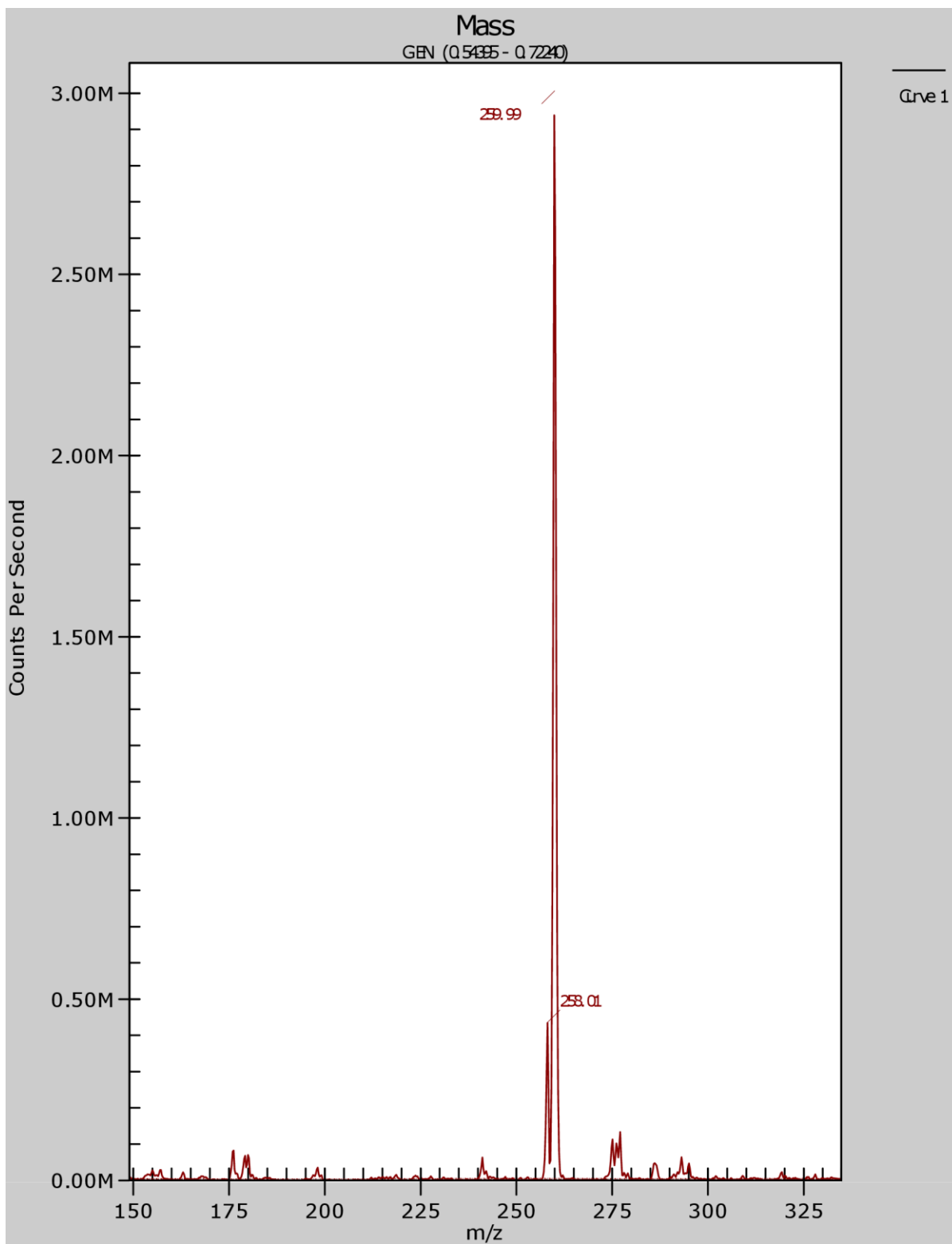


**Figure S10.** ESI-Mass spectrum of the  $[\text{Co}(\text{4Ql-tpy})_2](\text{PF}_6)_3$  complex in acetonitrile.

## Supporting Information

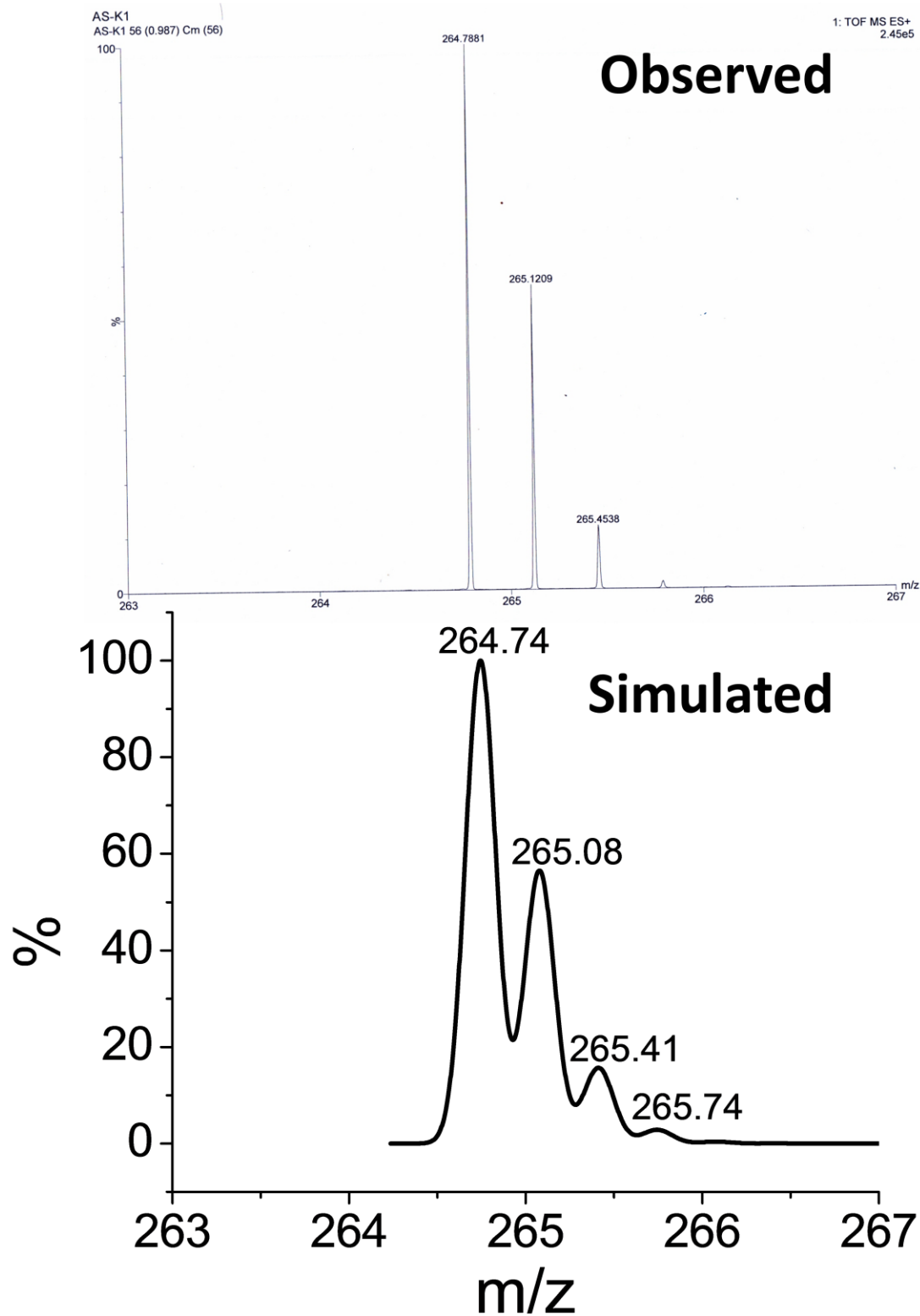


**Figure S11.** ESI-Mass spectrum of the  $[\text{Co}(4\text{-N-MeQl-tpy})_2](\text{PF}_6)_4$  complex in acetonitrile.

## Supporting Information

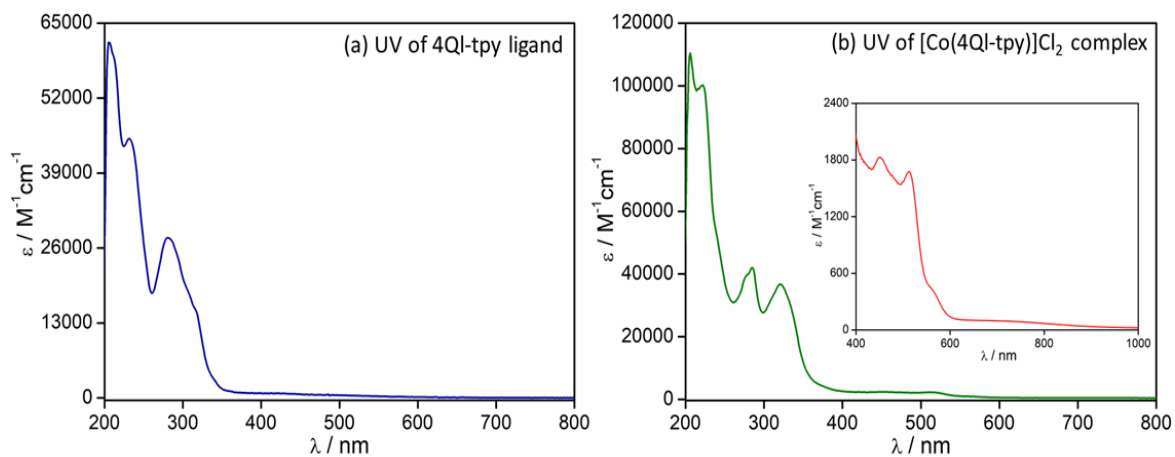


**Figure S12.** The UV-Vis spectrum of (a) ligand 4QI-tpy ( $1.25 \times 10^{-5}$  M) and (b)  $[\text{Co}(4\text{QI-tpy})_2]\text{Cl}_2$  complex ( $1.25 \times 10^{-5}$  M), inset shows the spectra for 1mM complex in methanol.

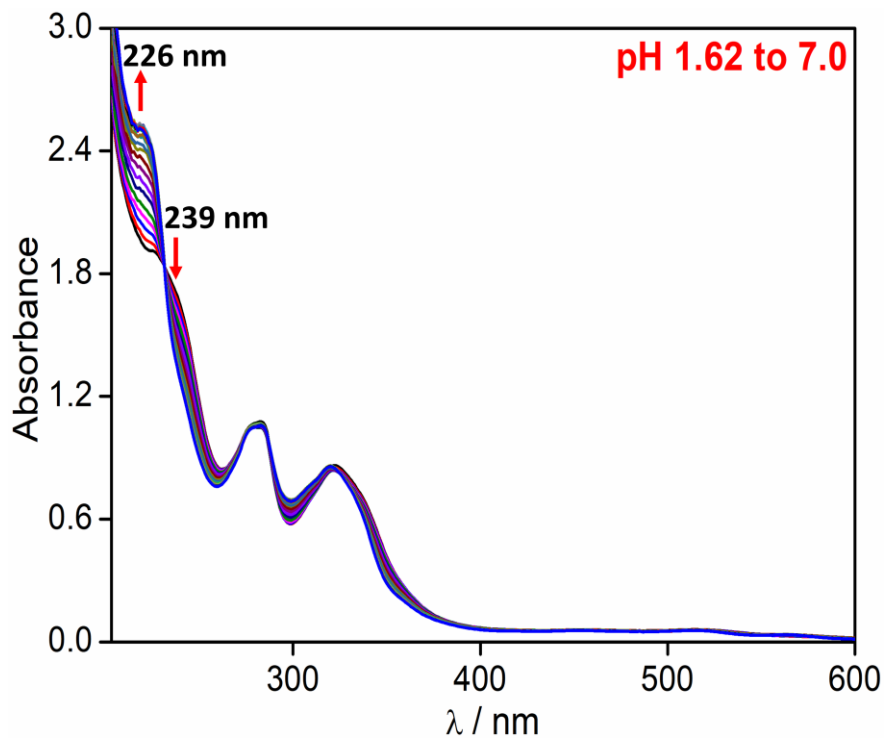


**Figure S13.** Change in UV-Vis spectra of  $[\text{Co}(4\text{QI-tpy})_2]\text{Cl}_2$  complex in phosphate buffer from pH 1.6-7.0.

## Supporting Information

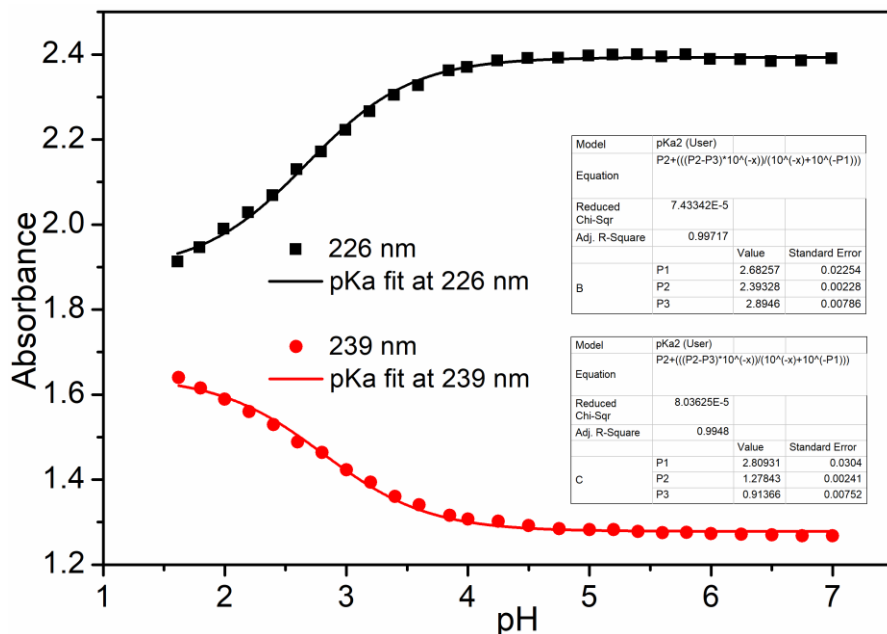


**Figure S14.** Absorbance vs. pH of  $[\text{Co}(\text{4Ql-tpy})_2]\text{Cl}_2$  complex in phosphate buffer from pH 1.62 - 7.0.

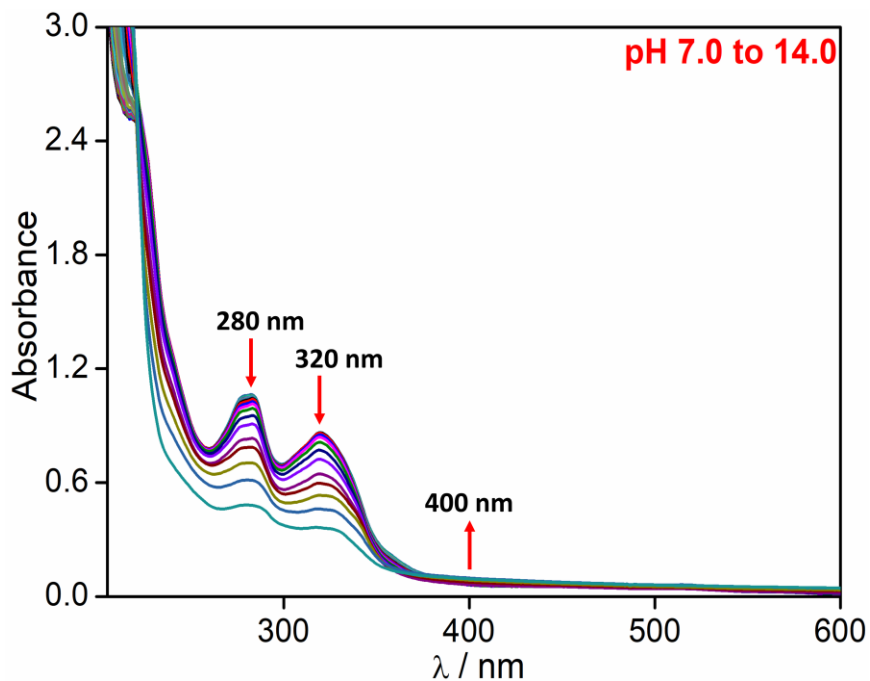


**Figure S15.** Change in UV-Vis spectra of  $[\text{Co}(\text{4Ql-tpy})_2]\text{Cl}_2$  complex in phosphate buffer from pH 7.0-14.0.

## Supporting Information

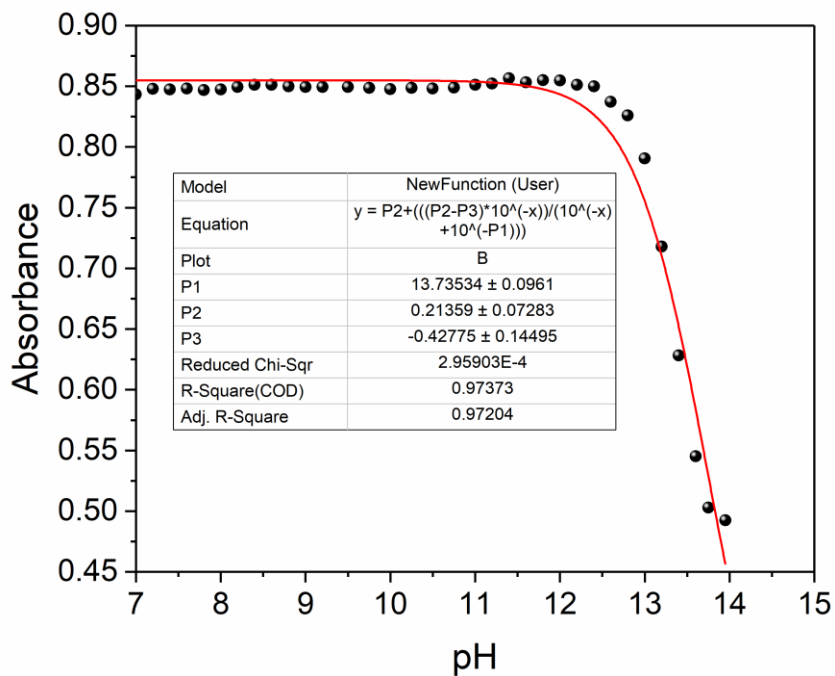


**Figure S16.** Absorbance vs. pH of  $[\text{Co}(\text{4Ql-tpy})_2]\text{Cl}_2$  complex in phosphate buffer from pH 7.0 – 14.0 at 320 nm.

## Supporting Information

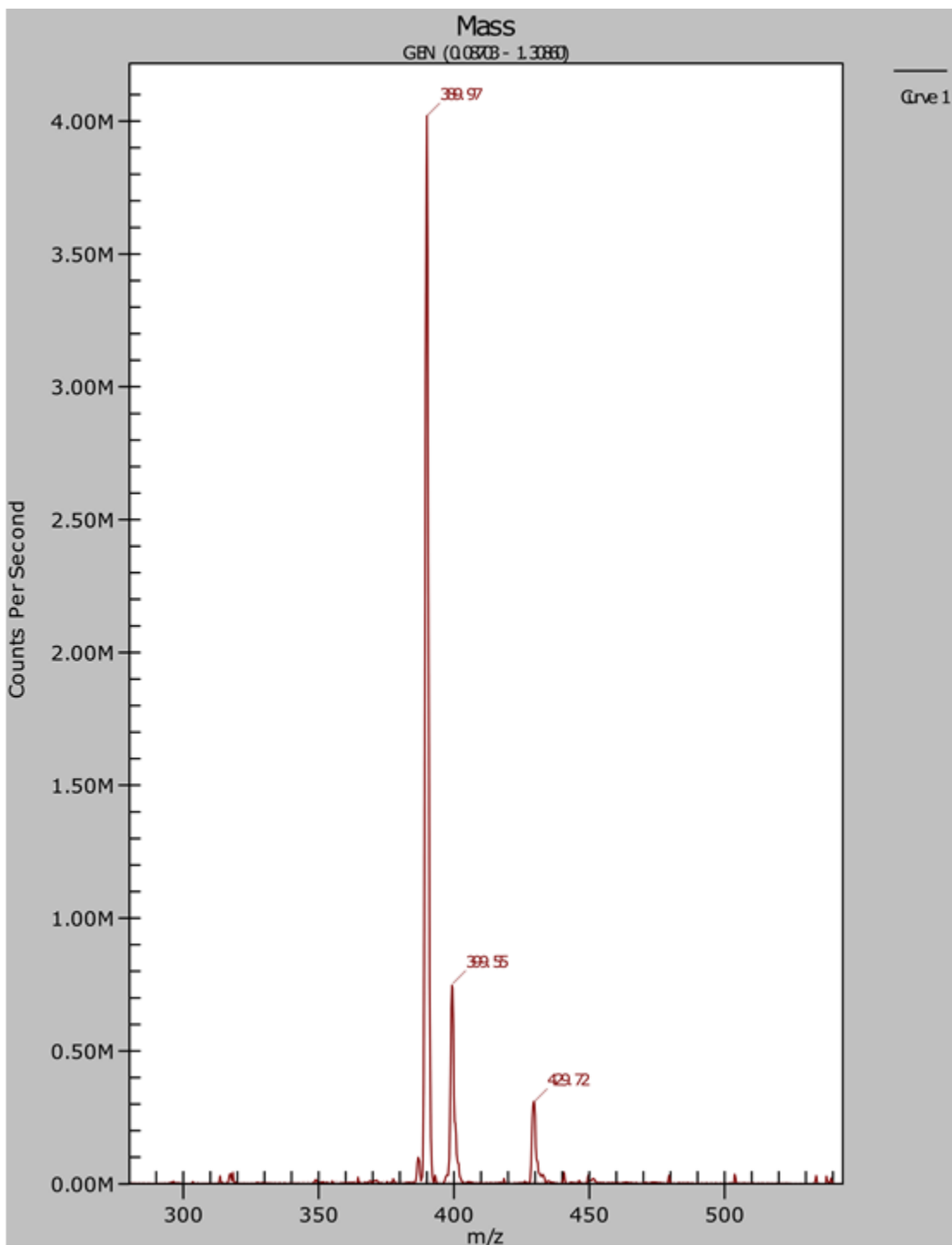


**Figure S17.** ESI-Mass spectrum of  $[\text{Co}(\text{4QI-tpy})_2]\text{Cl}_2$  in pH 7.0 phosphate buffer.

## Supporting Information

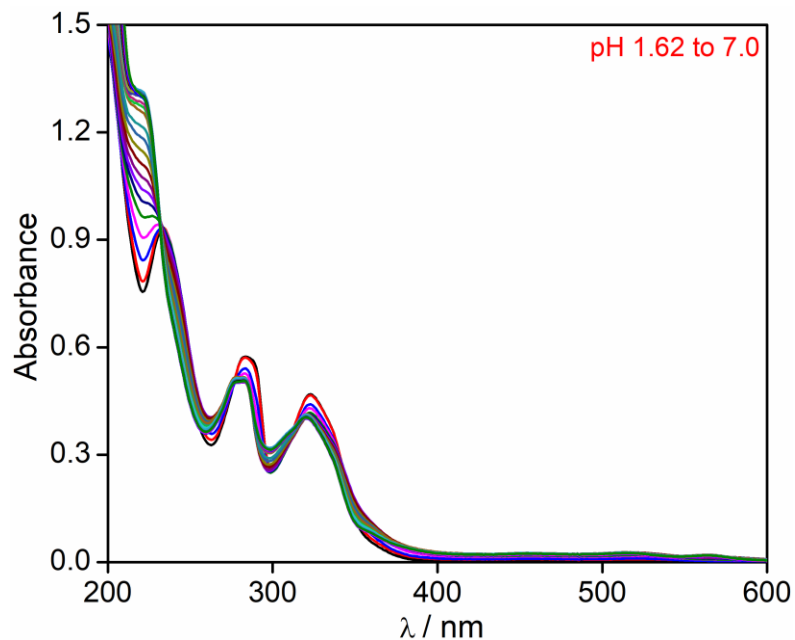


**Figure S18.** Change in UV-Vis spectra of  $[\text{Co}(\text{Me4Ql-tpy})_2](\text{PF}_6)_4$  complex in phosphate buffer from pH 1.62 to 7.0.

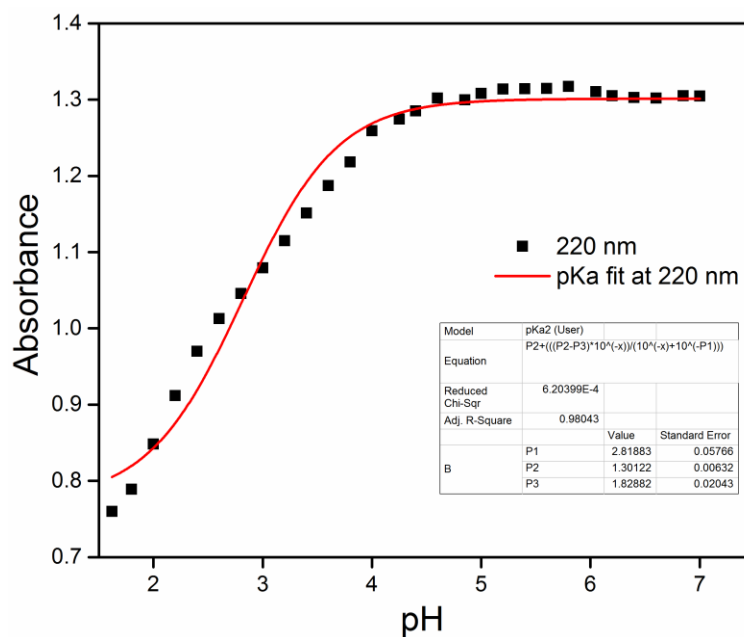


**Figure S19.** Absorbance vs. pH of  $[\text{Co}(\text{Me4Ql-tpy})_2](\text{PF}_6)_4$  complex in phosphate buffer from pH 1.62 to 7.0 at 220 nm.

## Supporting Information

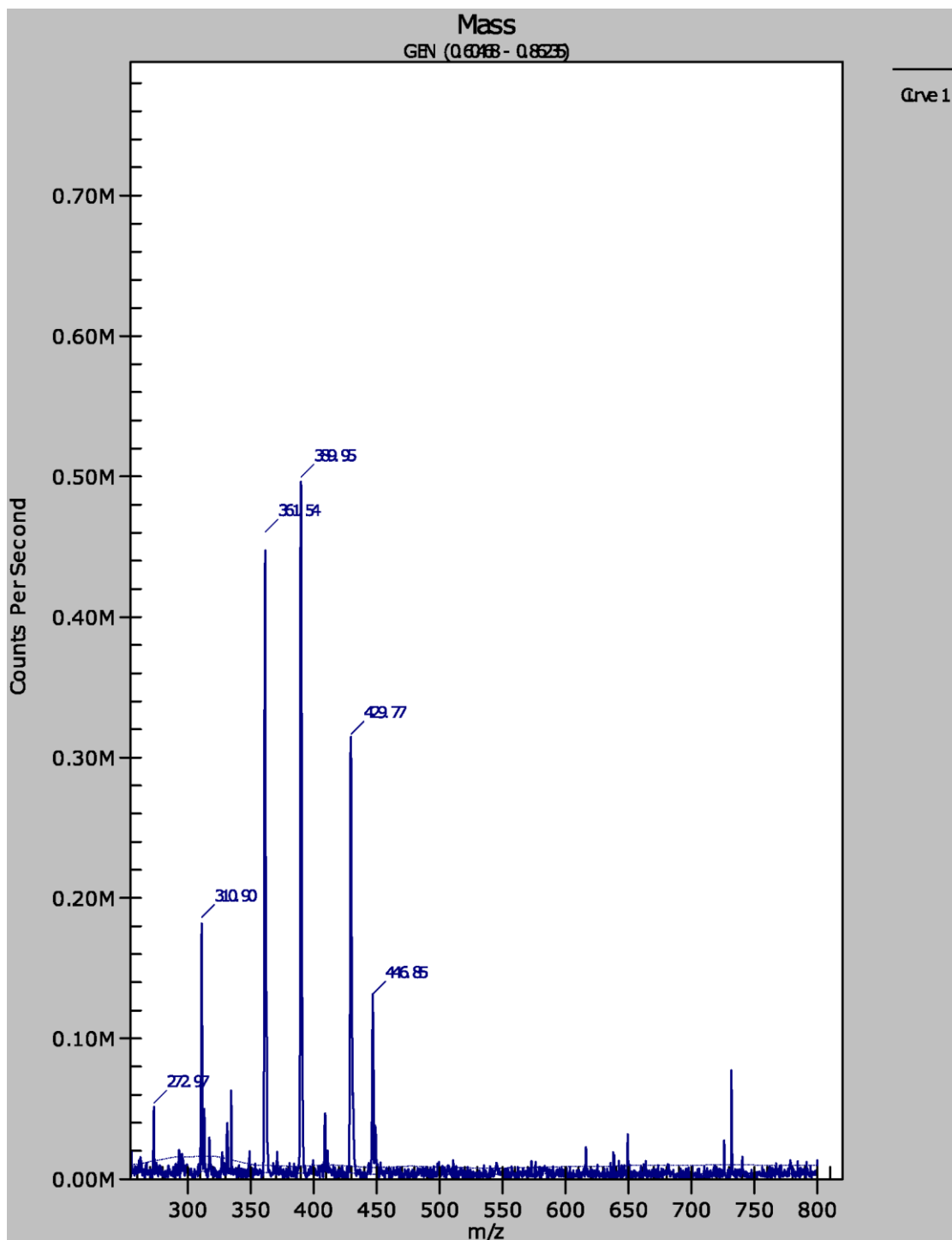


**Figure S20.** ESI-Mass spectrum of  $[\text{Co}(\text{4Ql-tpy})_2]\text{Cl}_2$  in pH 2.8 phosphate buffer.

## Supporting Information

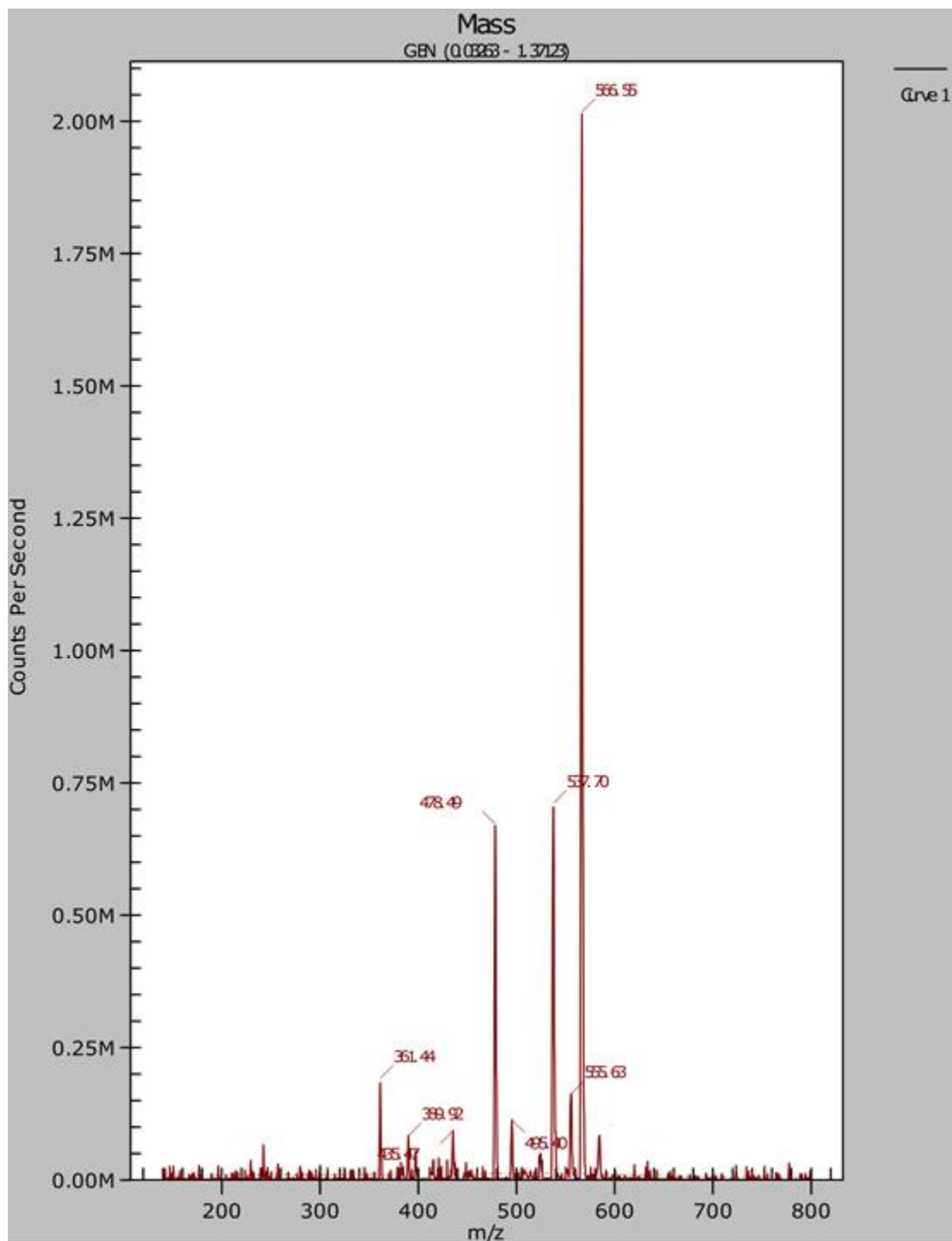


**Figure S21.** ESI-Mass spectrum of  $[\text{Co}(\text{4Ql-tpy})_2]\text{Cl}_2$  in presence of 30 equivalent of acetic acid.

## Supporting Information

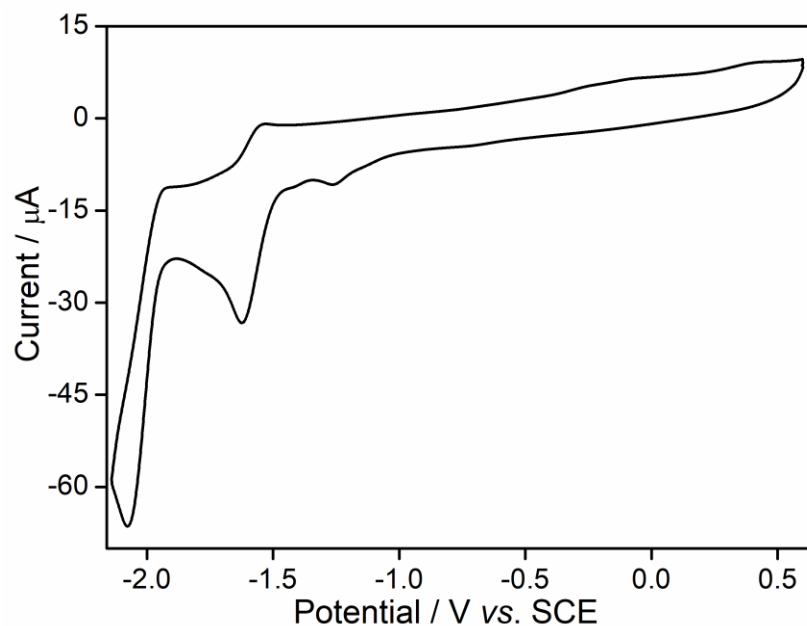


**Figure S22.** CV of 1 mM 4QI-tpy in DMF containing 0.1 M TBAP as supporting electrolyte and at a scan rate of  $100 \text{ mV s}^{-1}$  under inert atmosphere.

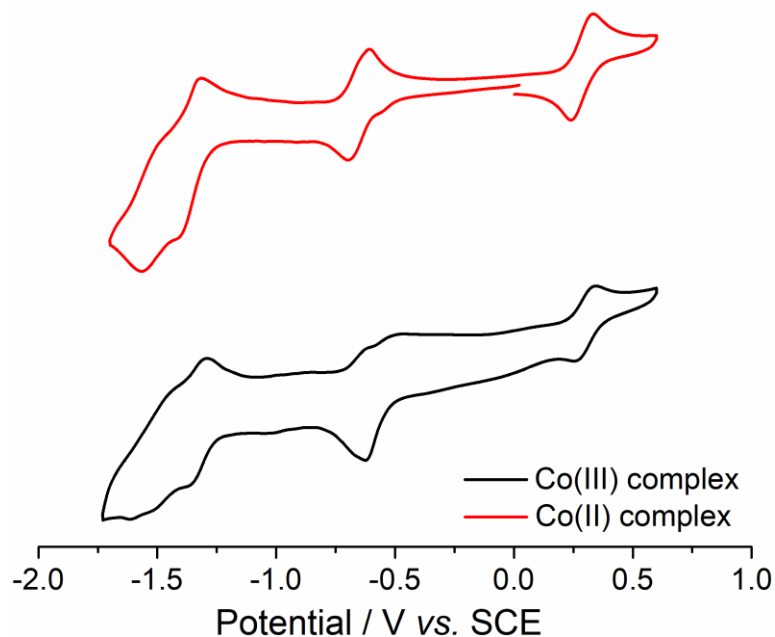


**Figure S23.** CV of 1 mM  $[\text{Co}^{\text{II}}(4\text{QI-tpy})_2]^{2+}$  and  $[\text{Co}^{\text{III}}(4\text{QI-tpy})_2]^{3+}$  in DMF containing 0.1 M TBAP as supporting electrolyte at a scan rate of  $100 \text{ mV s}^{-1}$  under  $\text{N}_2$  atmosphere.

## Supporting Information

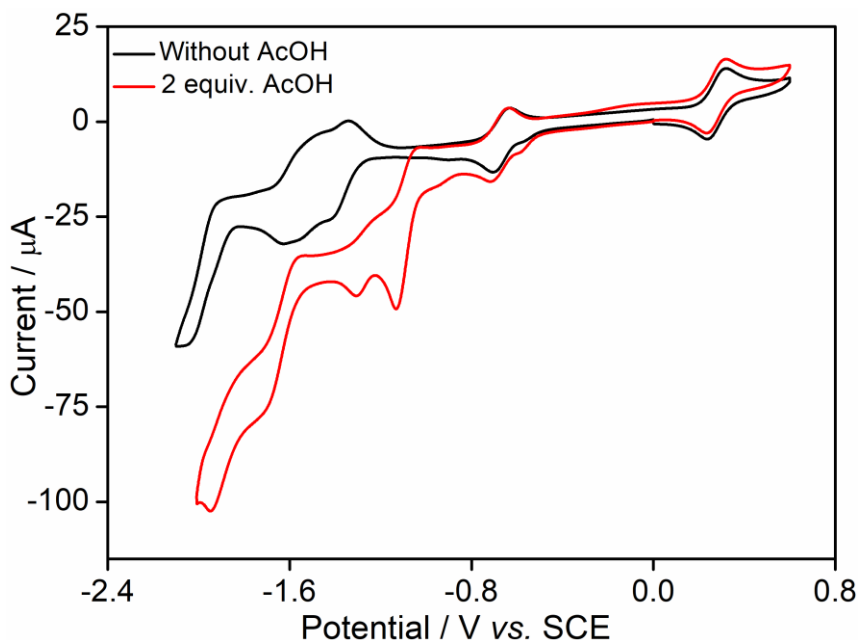


**Figure S24.** CV of 1 mM  $[\text{Co}(\text{4QI-tpy})_2]\text{Cl}_2$  in 95:5(v/v) DMF/ $\text{H}_2\text{O}$  with 0.1 M TBAP and an electrochemical potential scan rate of  $100 \text{ mV s}^{-1}$  in  $\text{N}_2$  atmosphere (black) and CV after addition of 2 equiv. of AcOH (red).

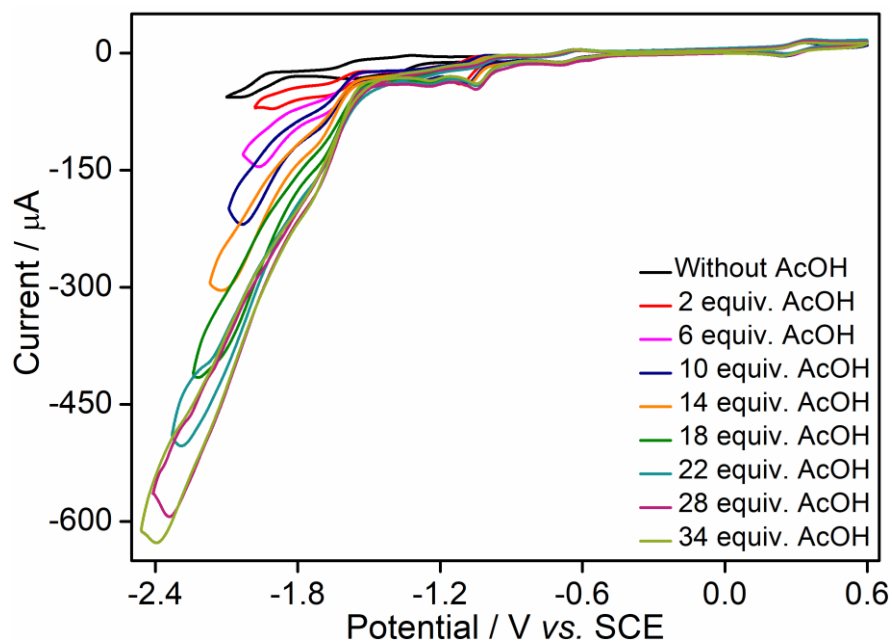


**Figure S25.** CV of 0.75 mM  $[\text{Co}(\text{4QI-tpy})_2]\text{Cl}_2$  in the presence of varying concentrations of acetic acid in DMF/ $\text{H}_2\text{O}$  (95:5, v/v) with 0.1 M TBAP at a scan rate of  $100 \text{ mV s}^{-1}$  under inert atmosphere.

## Supporting Information

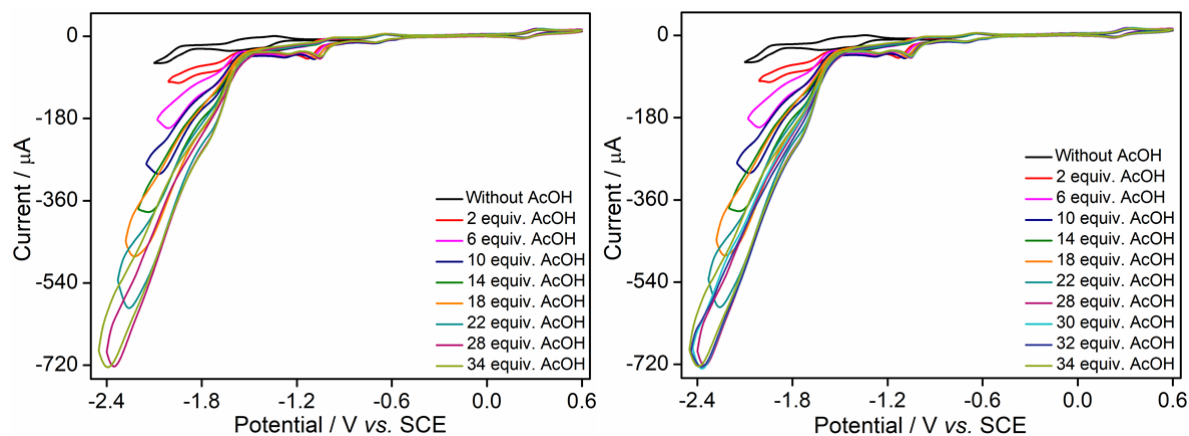


**Figure S26.** CV of 1 mM  $[\text{Co}(\text{4Ql-tpy})_2]\text{Cl}_2$  with varying concentration of AcOH in DMF/ $\text{H}_2\text{O}$  (95:5, v/v) and the supporting electrolyte TBAP (0.1 M) at a scan rate of  $100 \text{ mV s}^{-1}$  under  $\text{N}_2$  atmosphere (left). Right side CV shows the saturation after 28 equivalent of acetic acid.

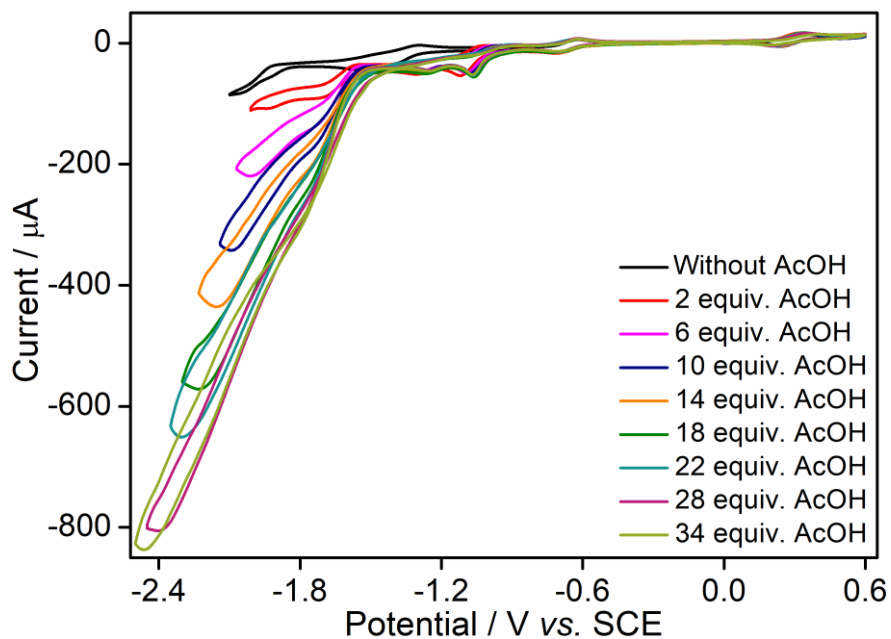


**Figure S27.** CV of 1.25 mM  $[\text{Co}(\text{4Ql-tpy})_2]\text{Cl}_2$  in the presence of varying concentrations of acetic acid in DMF/ $\text{H}_2\text{O}$  (95:5, v/v) with 0.1 M TBAP at a scan rate of  $100 \text{ mV s}^{-1}$  under inert atmosphere.

## Supporting Information

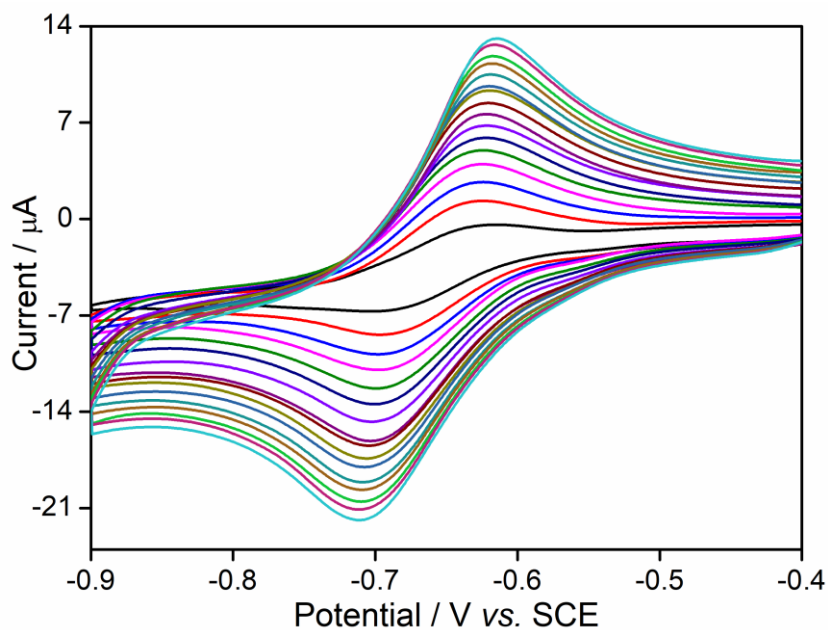


**Figure S28.** Cyclic voltammograms of 1mM [Co(4QI-tpy)<sub>2</sub>]Cl<sub>2</sub> in presence of 0.1 M TBAP in DMF/H<sub>2</sub>O (95:5, v/v) at varying scan rates from 25 - 400 mV/s.

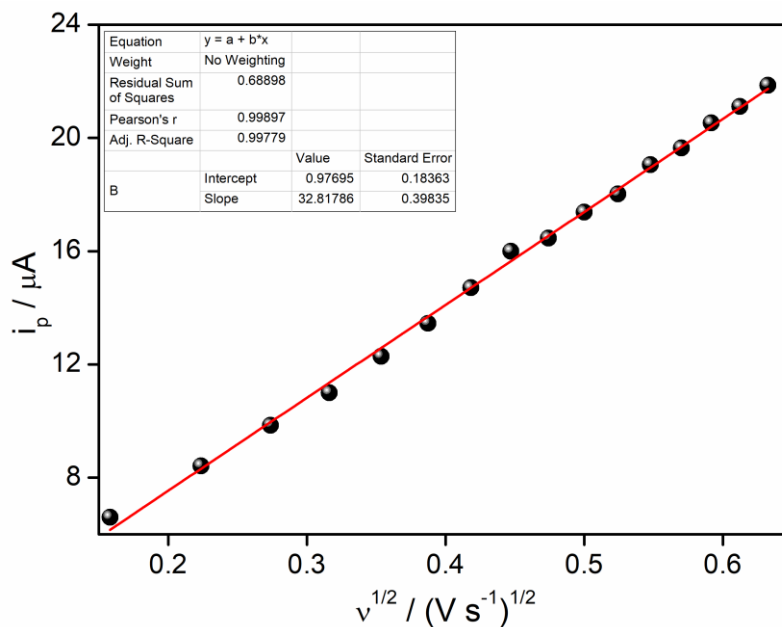


**Figure S29.** Plot of *i*<sub>p</sub> vs. *v*<sup>1/2</sup> with linear fitted slope  $3.2 \times 10^{-5} \text{ AV}^{-1/2} \text{ s}^{1/2}$ .

## Supporting Information

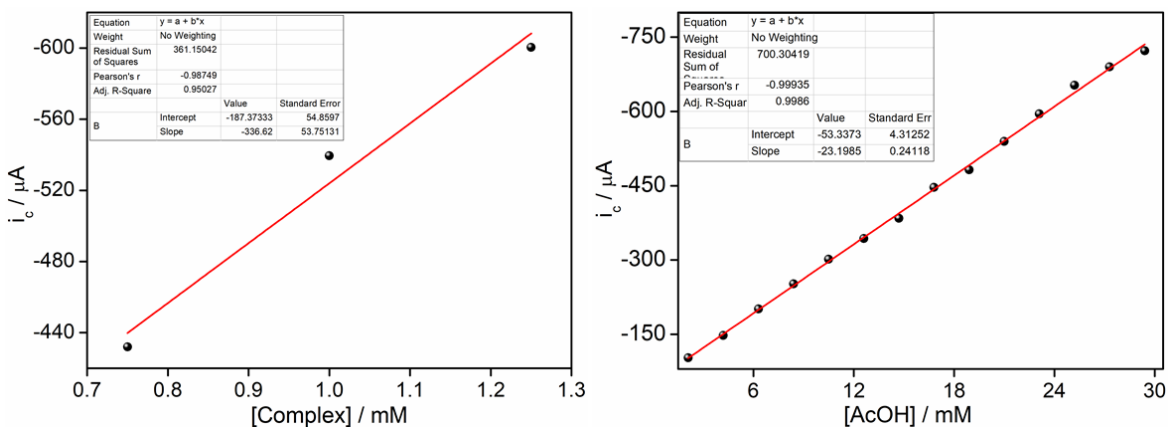


**Figure S30.** Dependence of catalytic current,  $i_c$  (a) on complex concentration in presence of 20 equivalent of acetic acid. (b) On acetic acid concentration for a catalyst concentration of 1.0 mM in potential scan rate of  $100 \text{ mV s}^{-1}$ .

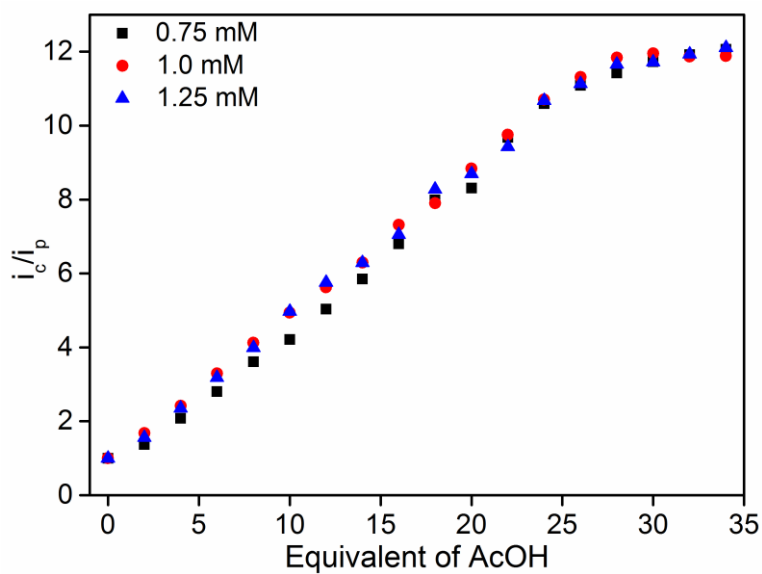


**Figure S31.** Dependence of  $i_c/i_p$ , on [AcOH] in three different concentrations of the catalyst (0.75 mM, 1.0 mM and 1.25 mM).

## Supporting Information

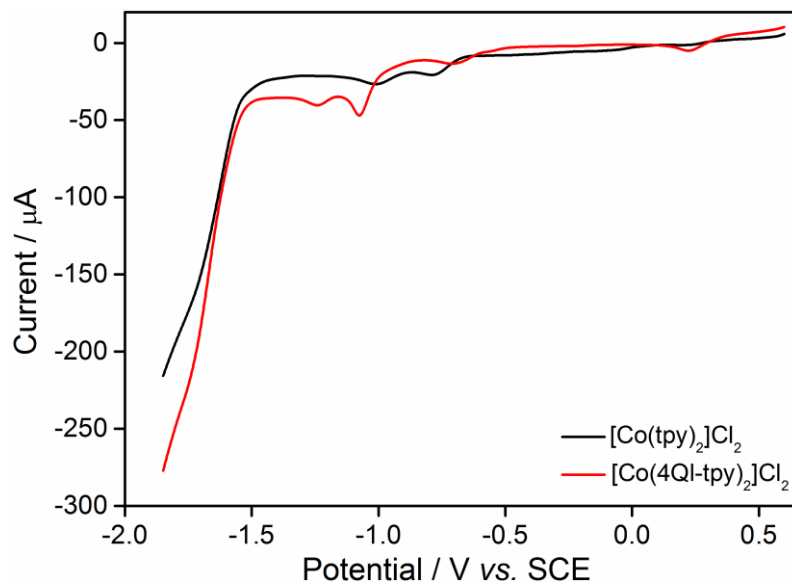


**Figure S32.** The linear sweep voltammogram (LSV) of  $[\text{Co}(\text{tpy})_2]\text{Cl}_2$  (black) and  $[\text{Co}(4\text{QI-tpy})_2]\text{Cl}_2$  (red) with the addition of 26 equiv. AcOH.

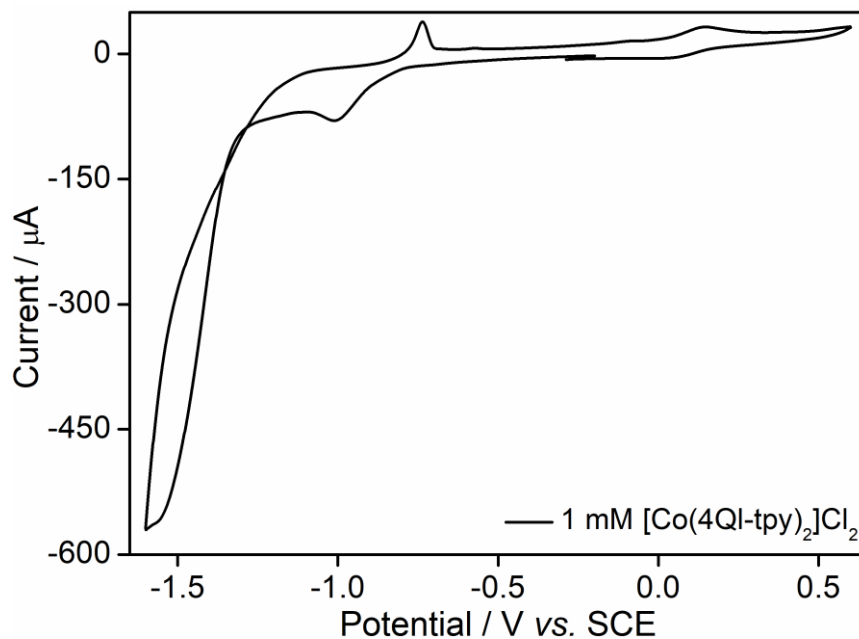


**Figure S33.** Cyclic voltammogram 1mM  $[\text{Co}(4\text{QI-tpy})_2]\text{Cl}_2$  in 0.1 M phosphate buffer at pH 7.0 using three electrode system in nitrogen atmosphere.

## Supporting Information

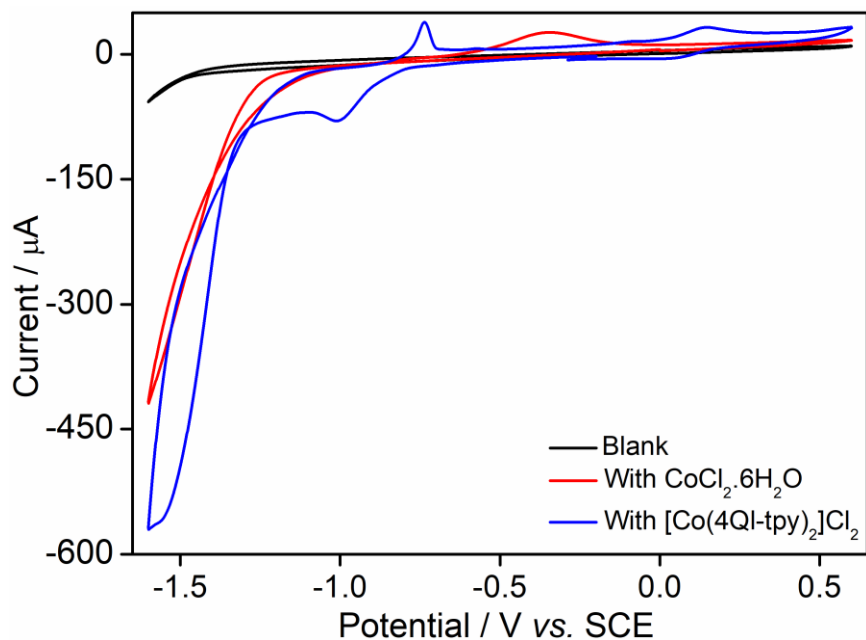


**Figure S34.** Cyclic voltammogram of blank (black),  $\text{CoCl}_2 \cdot 6\text{H}_2\text{O}$  (red) and 1mM complex (blue) in phosphate buffer of pH 7.0.

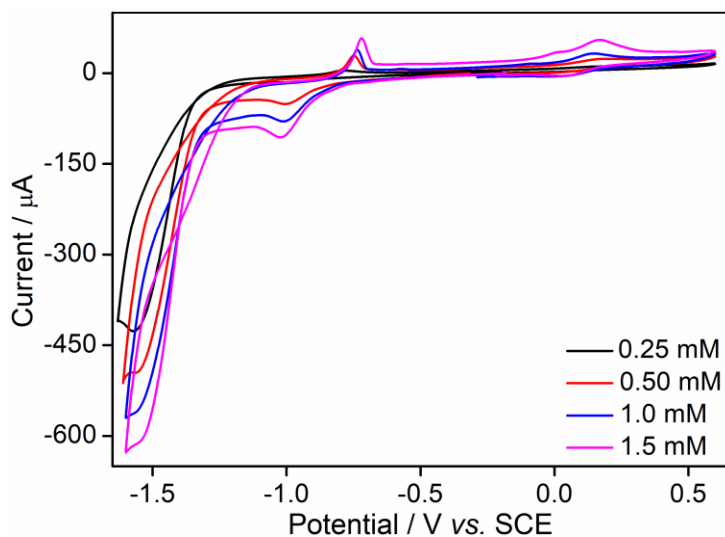


**Figure S35.** CV of  $[\text{Co}(\text{4QI-tpy})_2]\text{Cl}_2$  at various concentration (0.25 mM to 1.5 mM) at pH 7.0 in phosphate buffer (0.1 M) and  $\nu = 100 \text{ mV s}^{-1}$ .

## Supporting Information

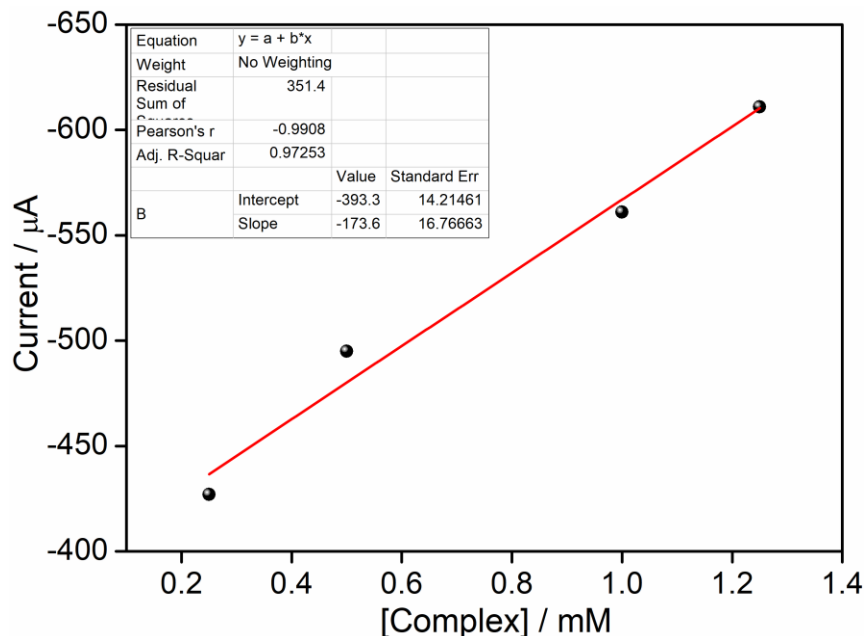


**Figure S36.** Variation of catalytic current ( $i_c$ ) with varying concentration of catalyst  $[\text{Co}(\text{4QI-tpy})_2]\text{Cl}_2$ .

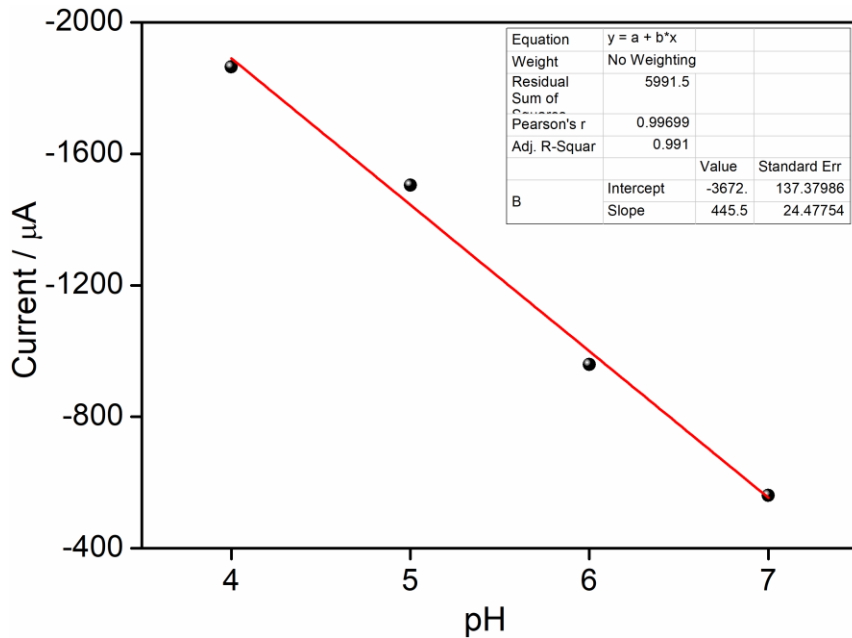


**Figure S37.** Variation of catalytic current ( $i_c$ ) of catalyst  $[\text{Co}(\text{4QI-tpy})_2]\text{Cl}_2$  with variation of pH.

## Supporting Information

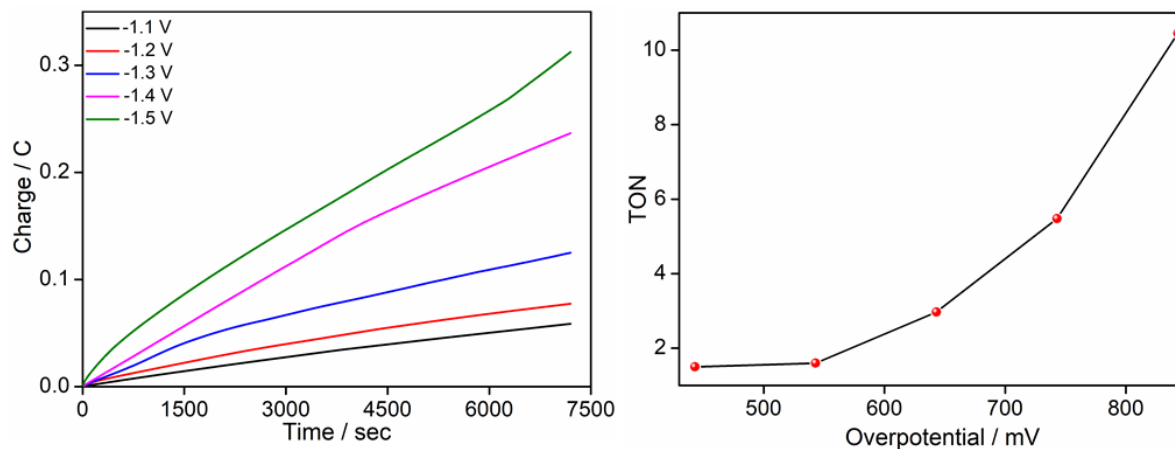


**Figure S38.** Charge build up during the time of electrolysis of  $5 \times 10^{-5}$  M  $[\text{Co}(\text{4Ql-tpy})_2]\text{Cl}_2$  in 0.1 M phosphate buffer of pH 7.0 with varying potential from -1.1 V to -1.5 V vs. SCE.

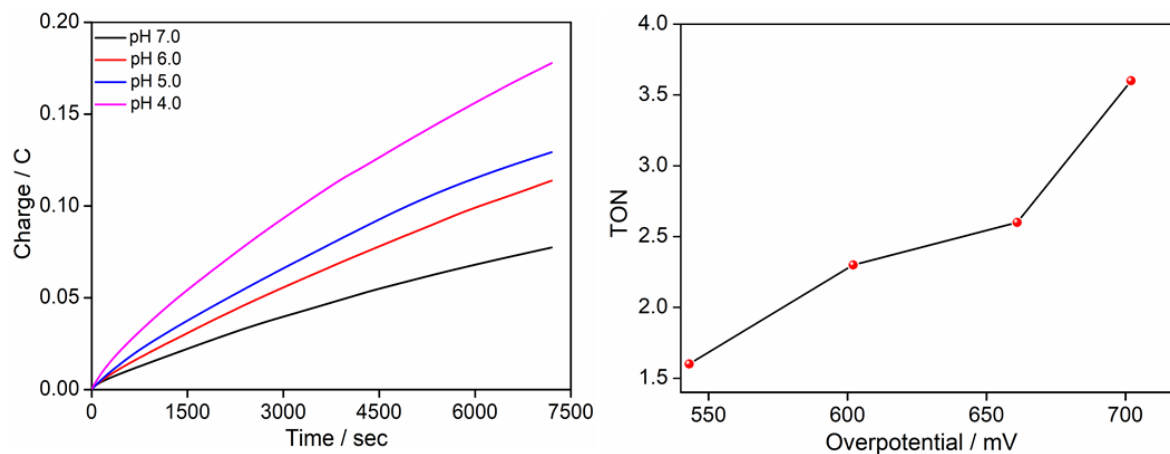


**Figure S39.** Charge build up during the time of electrolysis of  $5 \times 10^{-5}$  M  $[\text{Co}(\text{4Ql-tpy})_2]\text{Cl}_2$  in 0.1 M phosphate buffer with varying of pH 7.0 (pH 4.0 to pH 7.0) at potential of -1.2 V vs. SCE.

## Supporting Information

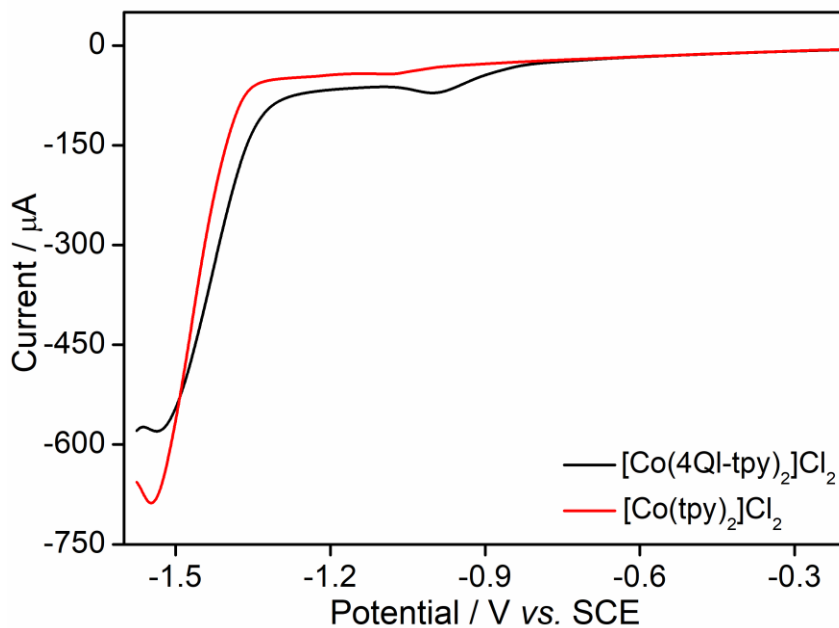


**Figure S40.** Linear sweep voltammogram of 1 mM  $[\text{Co}(4\text{QI-tpy})_2]\text{Cl}_2$  (black) and  $[\text{Co}(\text{tpy})_2]\text{Cl}_2$  in phosphate buffer at pH 7.0.

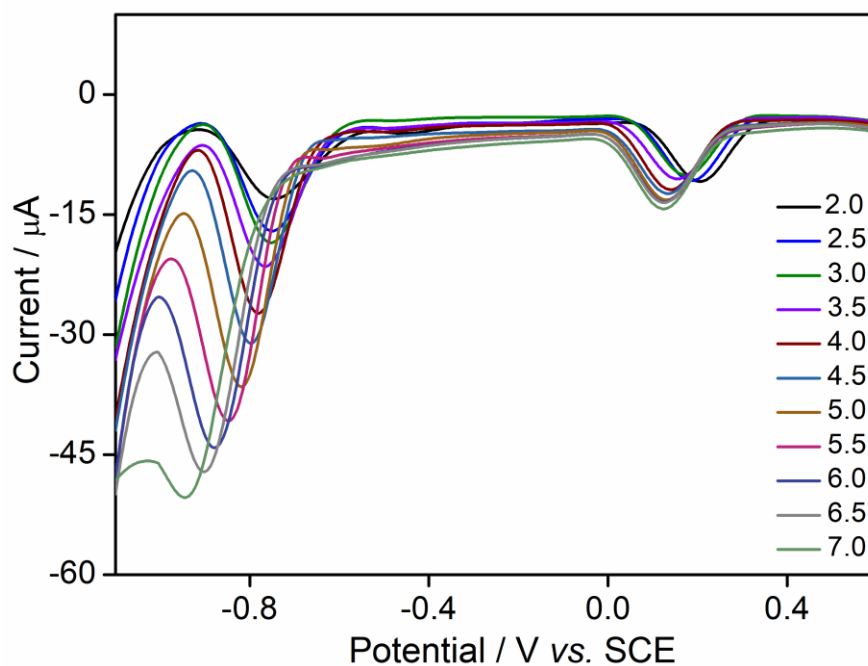


**Figure S41.** Change in DPV of  $[\text{Co}(4\text{QI-tpy})_2]\text{Cl}_2$  in Britton–Robinson buffer.

## Supporting Information

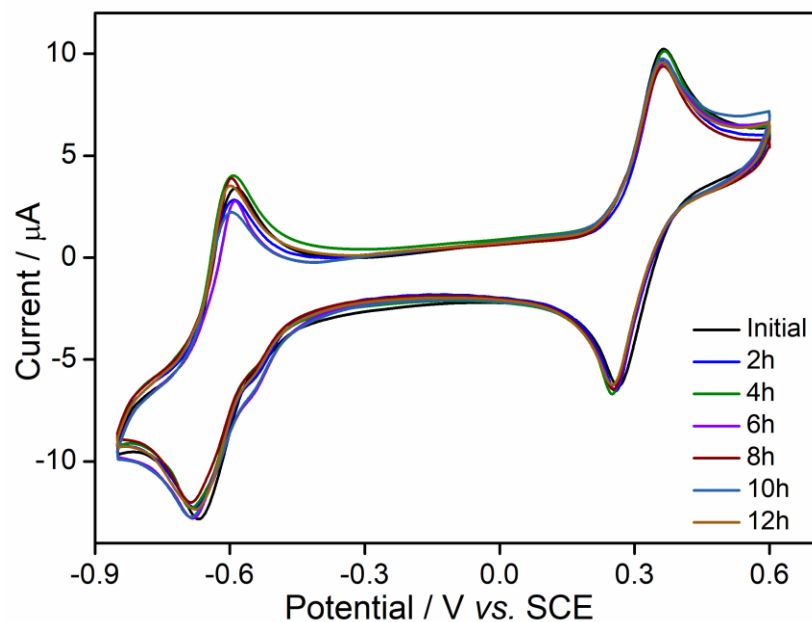


**Figure S42.** Time dependent cyclic voltammogram of  $[\text{Co}(\text{4QI-tpy})_2]\text{Cl}_2$  complex (1 mM) in DMF/ $\text{H}_2\text{O}$  (95:5, v/v).

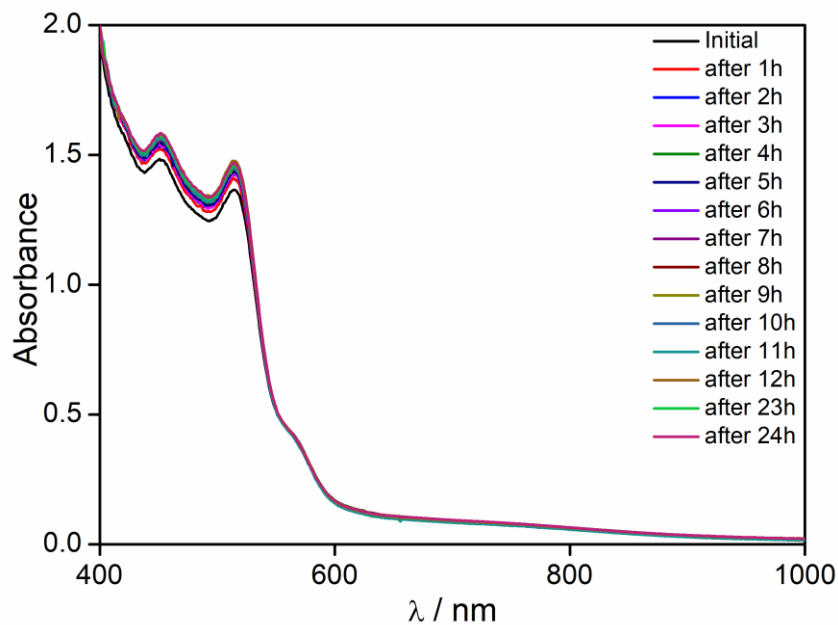


**Figure S43.** Time dependent UV-Vis spectra of  $[\text{Co}(\text{4QI-tpy})_2]\text{Cl}_2$  complex (0.75 mM) in DMF/ $\text{H}_2\text{O}$  (95:5, v/v).

## Supporting Information

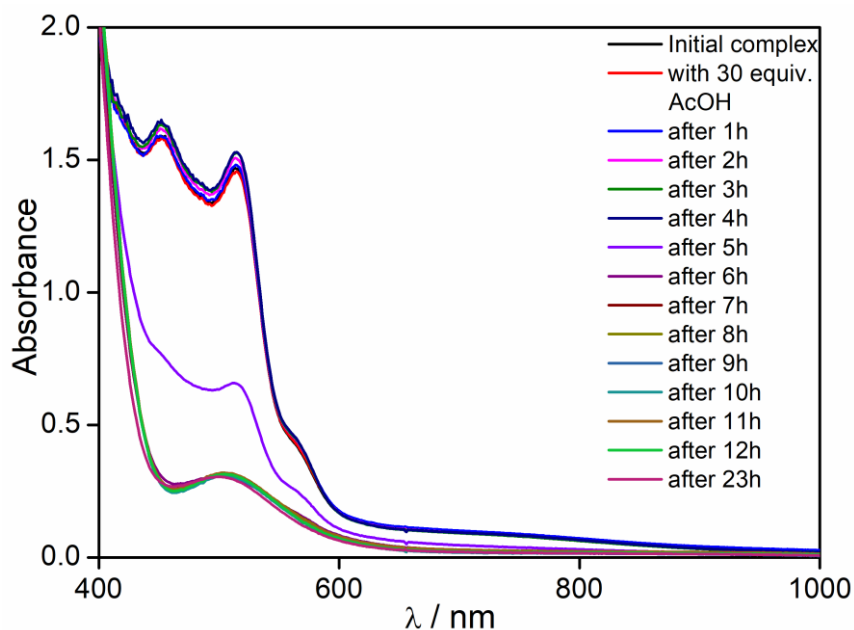


**Figure S44.** Time dependent UV-Vis spectra of [Co(4Ql-tpy)<sub>2</sub>]Cl<sub>2</sub> (0.75 mM) in DMF/H<sub>2</sub>O (95:5, v/v) in presence of 28 equiv. AcOH.

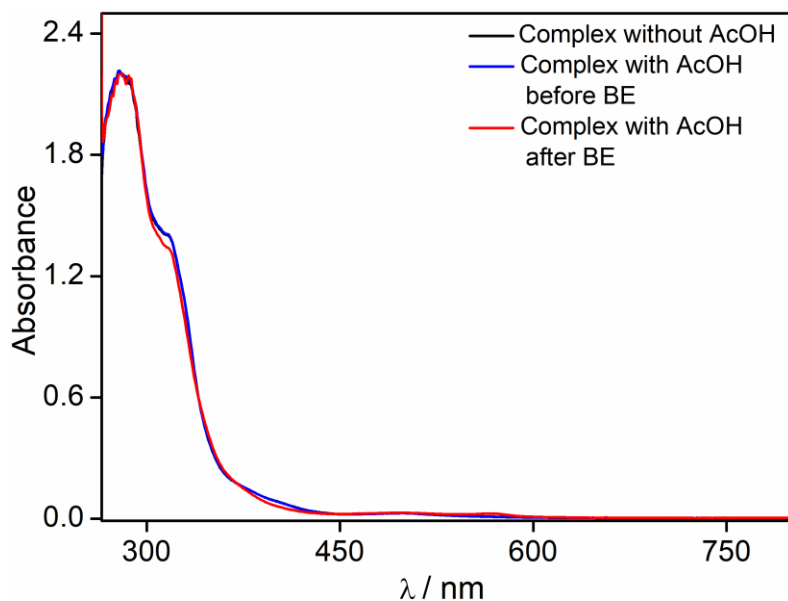


**Figure S45.** UV-Vis spectra of the  $5 \times 10^{-5}$  M [Co(4Ql-tpy)<sub>2</sub>]Cl<sub>2</sub> complex before and after the electrolysis (electrolysis at -1.6 V vs. SCE for 2 h) in presence of 28 equiv. AcOH in 95:5 DMF/H<sub>2</sub>O containing 0.1 M TBAP as a supporting electrolyte.

## Supporting Information

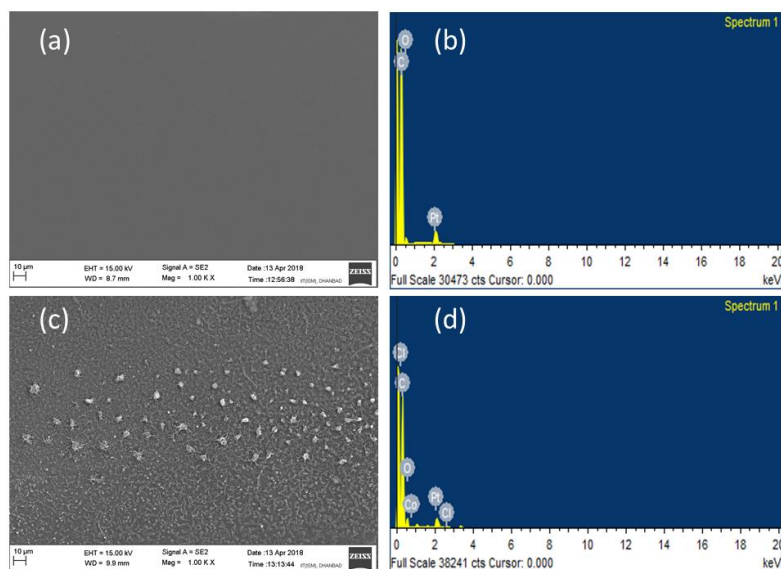


**Figure S46.** FESEM image of glassy carbon plate (a) before bulk electrolysis and (c) after bulk electrolysis of 2 hours at -1.6 V vs. SCE. EDX data of glassy carbon plate (b) before bulk electrolysis and (d) after bulk electrolysis of 2 hours at -1.6 V vs. SCE. Electrolysis condition: 0.05mM  $[\text{Co}(\text{4QI-tpy})_2]\text{Cl}_2$  with 28 equivalent acetic acid in DMF/ $\text{H}_2\text{O}$  (95:5, v/v) using 0.1 M TBAP as supporting electrolyte.

## Supporting Information

<b>Table S1. Crystal data and structure refinement for [Co(4Ql-tpy)<sub>2</sub>]Cl<sub>2</sub></b>	
Identification code	CCDC 1863596
Empirical formula	C <sub>96</sub> H <sub>76</sub> Cl <sub>4</sub> Co <sub>2</sub> N <sub>16</sub> O <sub>7</sub>
Formula weight	1825.39
Temperature/K	293.0
Crystal system	triclinic
Space group	P $\bar{1}$
a/Å	8.9073(6)
b/Å	12.9124(4)
c/Å	21.2304(6)
$\alpha$ /°	94.018(3)
$\beta$ /°	100.907(4)
$\gamma$ /°	100.487(4)
Volume/Å <sup>3</sup>	2343.79(19)
Z	1
$\rho_{\text{calc}}$ g/cm <sup>3</sup>	1.293
$\mu$ /mm <sup>-1</sup>	0.530
F(000)	942.0
Crystal size/mm <sup>3</sup>	0.21 × 0.19 × 0.16
Radiation	MoK $\alpha$ ( $\lambda$ = 0.71073)
2 $\theta$ range for data collection/°	3.22 to 54.9
Index ranges	-11 ≤ h ≤ 11, -16 ≤ k ≤ 16, 0 ≤ l ≤ 27
Reflections collected	10724
Independent reflections	10724 [R <sub>int</sub> = 0.0000, R <sub>sigma</sub> = 0.0037]
Data/restraints/parameters	10724/0/575
Goodness-of-fit on F <sup>2</sup>	1.090
Final R indexes [I ≥ 2 $\sigma$ (I)]	R <sub>1</sub> = 0.0695, wR <sub>2</sub> = 0.2005
Final R indexes [all data]	R <sub>1</sub> = 0.0696, wR <sub>2</sub> = 0.2006
Largest diff. peak/hole / e Å <sup>-3</sup>	0.67/-0.75